Optimal electric bus fleet scheduling considering battery degradation and non-linear charging profile

N.B. When citing this work, cite the original published paper.

(article starts on next page)
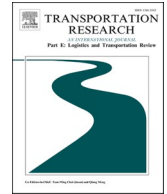
Optimal electric bus fleet scheduling considering battery degradation and non-linear charging profile☆

Le Zhang [a,c], Shuaian Wang [b], Xiaobo Qu [c,*]

[a] *School of Economics and Management, Nanjing University of Science and Technology, Nanjing 210094, China*
[b] *Department of Logistics and Maritime Studies, Hong Kong Polytechnic University, Hung Hom, Hong Kong*
[c] *Department of Architecture and Civil Engineering, Chalmers University of Technology, Gothenburg 41296, Sweden*

A B S T R A C T

This study aims to determine the battery electric bus service and charging strategy to minimize the total operational cost of transit system, where the cost incurred by battery degradation and non-linear charging profile is taken into account. We formulate a set partitioning model for this problem, subject to predefined trip schedule and limited charging facilities. A tailored branch-and-price approach is then proposed to find the global optimal solution. In particular, we develop an effective multi-label correcting method to deal with the pricing problem (i.e., generating columns) in column generation procedure within the branch-and-price framework, coupled with a dual stabilization technique with an aim to accelerate the convergence rate. Meanwhile, a branch-and-bound solution approach is adopted to guarantee optimal integer solutions. Numerical experiments and a case study arising from real transit network are conducted to further assess the efficiency and applicability of the proposed method. Our experiments confirm that, despite the complexity of the considered problem, optimal solution can still be generated within reasonable computational time using the proposed algorithm. The results also show considerable cost saving (about 10.1–27.3% less) if this optimization model is implemented, mainly contributed by the substantial extension of battery life. A number of managerial insights stemmed from the numerical case study are outlined, which can help transit operators formulate more cost-efficient electric bus fleet scheduling plans.

1. Introduction

With local government in many countries implementing a range of policies (e.g., financial incentives, customer subsidies, and taxes on petroleum) to facilitate the introduction of electric vehicles, more and more transit operators begin to use battery electric buses (BEBs) to provide public service (Nie et al., 2016). In recent years, we have witnessed rapid market-share growths of BEBs in transit system. For example, in the year of 2016, the subsidy policy for BEBs named Elbusspremien was introduced in Sweden, where the bus companies and transit agencies could receive a discount of 20% in BEB's purchase prices (Skog and Arbresparr, 2017). Since then, the bus fleets were gradually replaced by BEBs in some Swedish cities, e.g., Umea and Goteborg. Shenzhen, one of the largest cities in China, replaced all of its diesel city buses with BEBs in 2017. It is predicted that the number of BEBs in service would triple from
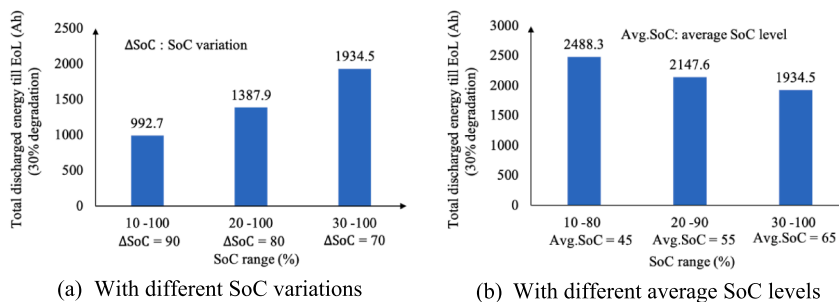

Fig. 1. Total discharged energy till EoL under different SoC ranges based on LiFePO$_4$ cells with a normal capacity of 1.1 Ah.

386,000 in 2017 to 1.2 million in 2025, accounting for 47 percent of the world's total city bus fleet (Chediak, 2018). Undoubtedly, transit electrification is becoming an unstoppable trend and BEB fleets will dominate the future of public transit due to their considerable advantages in terms of reducing air pollutant and efficient energy consumption (An, 2020; Bie et al., 2020; Ghamami et al., 2016; Gu et al., 2020; Pelletier et al., 2019; Qu et al., 2020; Qu and Wang, 2021).

Despite these advantages, the large-scale adoption of BEBs is still hampered by some technical constraints. BEBs typically involve much higher initial investment than conventional diesel buses, where the embedded battery packs are a major cost component. Even though the price of battery packs has been rapidly decreasing, a very significant portion of the bus cost can still be attributed to the battery (Nykvist and Nilsson, 2015). Moreover, battery capacity fades during charge and discharge cycling, and the battery performance degrades as consequence. The end of life (EoL) of a battery is reached when its available capacity under reference conditions has decreased to 70-80% of the initial value (Zhang et al., 2019). The battery packs in BEBs thus should be replaced periodically, which further decreases the attractiveness of BEBs (Pelletier et al., 2017; Schoch et al., 2018). Therefore, it is of utmost importance from a cost perspective to incorporate battery health considerations into scheduling schemes of BEBs. In addition, compared with conventional diesel buses, BEBs are still suffering from range anxiety problems and the limited travel range can further decline during operation due to battery capacity fading. Hence, BEBs usually cannot finish a whole day's operation without recharging—although their longest drive range under normal urban road conditions has reached 250 km when lithium-ion battery packs are used. The need to recharge the buses while maintaining existing service schedule with well-considered battery management makes emerging BEB service more challenging to some extent and creates additional managerial problems for transit operators (Li, 2013; Kang et al., 2015; Lebeau et al., 2016; Masmoudi et al., 2018). To address this dilemma and seize the market, a well-planned BEB scheduling with full consideration of battery health is thus crucial for the smooth operation of city BEBs. The relevant studies are scattered over a wide variety of journals spanning several research fields, including in particular the field of battery cells and transportation engineering.

Currently, lithium-ion batteries are widely used in modern electric vehicles due to their high energy density. In the field of battery cells, researchers have conducted numerous laboratory aging tests to study the capacity fading mechanism of lithium-ion batteries and proposed a variety of prediction models. Even though the model forms and model parameters vary largely over the cell materials and modeling approaches, similar conclusions can still be found for all types of lithium-ion batteries embedded in BEBs: operating conditions are the major stress factors for battery aging, which is related to time, energy throughput, temperature, and in particular the state of charge (SoC) (Lam and Bauer, 2012; Grolleau et al., 2014; Zhang et al., 2019). Let us use LiFePO$_4$[1] as an example. As per Fig. 1, we have 1) the total discharged energy till the EoL under a SoC variation from 100% to 10% is only half of that from 100% to 30%, as per the solid experimental data based on LiFePO$_4$ cells; 2) given the same SoC variation or cycling SoC swing, the total discharged energy is negatively related to the average SoC level (Lam and Bauer, 2012). It is worth to note that the SoC-dependent battery capacity fading mechanism revealed above is valid for all types of lithium-ion batteries (e.g., LiCoO$_2$, NCA, Li(NiCoAl)O$_2$ and LiFePO$_4$ cells): the higher either the SoC variation or average SoC level is, the faster battery capacity fades. Therefore, transit operators are suggested to keep the SoC of battery packs in a range that is as narrow as possible (i.e., smallest SoC variation) and at a low level (i.e., lowest average SoC level), which will substantially prolong battery lifespan and thus achieve cost saving in the long run. However, the need to constrain SoC within a narrow range and at a low level would influence the current BEB scheduling schemes and BEB fleet size as well, especially when charging facilities are limited. To the best of our knowledge, whereas much efforts have been made in the field of battery cells to study battery aging mechanism, no existing study has incorporated the above critical features in transport engineering studies.

From the perspective of transportation engineering, optimal scheduling of BEBs has attracted increasing attention in recent research and been extensively examined in the context of vehicle scheduling problem (VSP) (Li, 2013; Alder and Mirchandani, 2014; Wen et al., 2016; Wang et al., 2017; Li et al., 2018; Rinaldi et al., 2019) and vehicle routing problem (VRP) (Schneider et al., 2014; Keskin and Çatay, 2016; Hiermann et al., 2016; Montoya et al., 2016; Yi et al., 2018). In particular, for the specific instance of BEB scheduling, either route duration or route distance is constrained in the model. Meanwhile, the transit network is equipped with some charging points (i.e., public swapping and charging stations) where BEBs can be fully or partially replenished (Hof et al., 2017; Montoya et al., 2016; Adler and Mirchandani, 2014). These studies presented how to manage and schedule the full-BEB fleet or hybrid-

---

[1] LiFePO$_4$ cell is a type of lithium-ion battery.

BEB fleet to yield the least operational costs and reduce the overall pollutant emissions as well (Li, 2013; Li, 2016; Rinaldi et al., 2019). For example, Li (2013) proposed a vehicle-scheduling model for BEBs with either battery swapping or fast charging to minimize total operational cost subject to predefined trip schedule, while Rinaldi et al. (2019) focused on the optimal scheduling of mixed BEB fleet. Unfortunately, due to complexity of electrochemical properties in lithium-ion batteries, very little attention has been dedicated to explicitly considering battery health in BEB scheduling. What is more, to remedy the range anxiety problem, recent studies in electric vehicle scheduling usually require charging the battery in full, which would lead to larger SoC variation, higher average discharge interval, and subsequently higher capacity fading rate (Schneider et al., 2014; Hiermann et al., 2016). Empirical evidence from field trials also shows that majority of transit operators prefer to reconnect the BEBs for full charging overnight to have the full range available in the next day. Although this frequent full-charging behavior could minimize the drivers' anxiety, this benefit is achieved at the cost of shortening battery's lifetime. Hence, the joint consideration of BEB service schedule, charging strategy, and their impact on battery capacity fading is essential in terms of prolonging the battery lifetime and minimizing total operational cost.

In addition, the electrochemical properties of batteries suggest that SoC increases nonlinearly with respect to the charging time. This nonlinear charging profile is another feature of utmost importance whilst was paid little attention to by transport planning community. In general, the battery level increases concavely with charging time, instead of linearly, because the terminal voltage and current vary during the charging process (Pelletier et al., 2017). Assuming linearly charging profile would overrate the charging efficiency and lead to the underestimation of the fleet size of BEBs (Montoya et al., 2017; Xu and Meng, 2019). In this study, we will bridge the research gap as well by incorporating the nonlinear charging profile into the fleet size determination for BEB transit service.

In light of the above, there is a need for further development in BEB scheduling problem, regarding how to take certain fundamental battery characteristics into account. In this paper, we will advance the research frontier by incorporating battery management into the optimization framework of BEB scheduling. To be specific, we focus on examining how to best schedule BEBs to serve the trips originating from and returning to a single central terminal. Our objective is to minimize the total operational cost by determining service sequence of BEBs, charging strategy and BEB fleet size, subject to limited charging facilities. To explicitly consider battery health in charging recommendations, the cost incurred by battery degradation is set as a primary objective, i.e., a major cost component of total operational cost. Meanwhile, realistic nonlinear charging profile and partial charging are well-considered in the optimization framework, which would make the decision-makings more complicated. To achieve this goal, a set partitioning model is built for the studied problem, and this modeling approach is widely adopted in some previous work in the context of VSP (Li, 2013; Xu and Meng, 2019). A tailored branch-and-price (B&P) approach is subsequently proposed to solve the model. To be specific, we firstly design a column generation (CG) procedure to solve the linear relaxation of the problem, coupled with a dual stabilization technique aimed at accelerating the convergence rate of the proposed algorithm. Then to guarantee feasible integer solutions, the CG procedure is embedded into a branch-and-bound (B&B) search framework. It is worth to note that, the solution approach is developed by fully taking advantage of the model's unique features, which will be described in detail over the following sections. The models and solution approach are tested through a large number of numerical experiments. The results unveil that by taking certain fundamental electrochemical properties of lithium-ion batteries into consideration, the optimal total cost can be saved by up to 10.1–27.3% and the battery's service life can be extended by additional 47.2–96.1% approximately.

Our key contributions from a theoretical and practical point of view can be summarized as follows:

(i) We are, to our best knowledge, the first to formulate and solve BEB scheduling problem that incorporates both battery health considerations and nonlinear charging profile into the optimization framework;

(ii) With full consideration of the problem's unique features, a specialized branch-and-price solution method is proposed to guarantee the global optimum of the model within moderate runtimes for real-life-scale instance;

(iii) A number of managerial insights stemmed from the numerical case study are outlined, which can serve as a solid theoretical foundation for more cost-efficient BEB service.

The rest of this paper is organized as follows. Section 2 presents the problem description. A set partitioning model for the studied problem is built in Section 3. Section 4 elaborates the proposed B&P approach for solving the problem. The computational efficiency of our approach is tested in Section 5. Numerical case studies are furnished in Section 6. Conclusions and potential extensions of the present work are discussed in Section 7.

2. Problem description

To explicitly elaborate a single-terminal BEB scheduling problem, several aspects of this problem will be covered in this section. To be specific, the single-terminal transit network, definition, feasibility and cost of a trip chain are described in Section 2.1. The battery degradation mechanism and the nonlinear charging profile of BEBs are presented in Sections 2.2 and 2.3 respectively. Following that, Section 2.4 summarizes the joint consideration of BEB scheduling and charging strategy. The notations used throughout this study are summarized in Appendix A.

2.1. Single-terminal transit network and trip chains

In this study, a single-terminal transit network is adopted to define the BEB scheduling problem, guaranteeing that a sequence of timetabled round-trips can be satisfied successfully, as shown in Fig. 2. The selected terminal is equipped with limited normal charging facilities and the capacity is denoted as C. The BEBs can be charged when parking at the terminal if there exist available charging
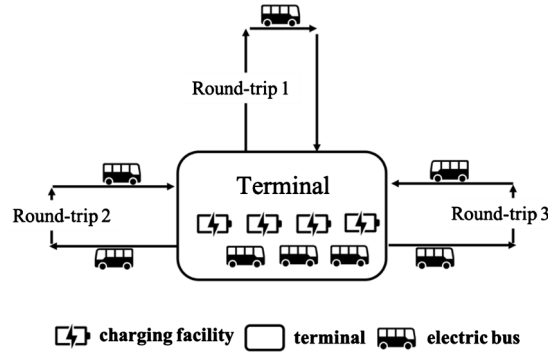
Fig. 2. Single-terminal transit network.

facilities. Such transit network is commonly used (e.g., Shenzhen city and Luxembourg city) and has been studied in a number of works in the context of bus scheduling (Kim and Schonfeld, 2013; Rinaldi et al., 2019). For simplicity, we will refer to the round-trip as trip for short from now on. Here we discretize time domain into consecutive time steps $t \in \{1, 2, \cdots, T\}$ with a discretization step as $\mathscr{L}$. All the trips, predefined by the transit planners, are grouped into a set denoted by I. For each trip $i \in I$, it is described by a triple $Q_i = \{s_i, e_i, m_i\}$, where s_i indicates the departure time [time step], e_i stands for the cycle (terminal to terminal) duration [time step], and m_i denotes the proportion of electricity consumed with respect to the maximum possible charge it can hold [%]. The above information for each trip $i \in I$ is deterministic and assumed to be known a priori. This assumption is acceptable for tactical decision-making problem targeted by this study. Also note that, for the ease of presentation, analogous to the expression of m_i, the amount of electricity replenished at terminal station is also expressed as the variation of electrical charge in percentage.

Let SoC_{init} denote the initial SoC of the BEB at the very beginning of daily operation period. It is defined as a model parameter in this study and its effect on the objective value will be carefully examined in the numerical cases. Throughout the paper, we adopt the assumption that the BEB is always charged to SoC_{init} whenever charging activity occurs during the daily operation period. In addition, at the end of daily operation, the BEB will be recharged back to SoC_{init} to prepare for the next day's service. This assumption is well in line with the empirically observed charging behaviors as it is convenient to apply and requires less organizational effort (Qin et al., 2016; Rinaldi et al., 2019). Also note that, in practice, BEBs are usually fully charged or near fully charged at the very beginning of daily operation period, because trip services are mostly concentrated during the daytime and BEBs can thus be charged overnight. Therefore, it is reasonable to constrain SoC_{init} by:

$$70\% \le SoC_{init} \le 100\% \tag{1}$$

Consider a transit operator who operates the daily public transport services using a fleet of homogeneous BEBs. To satisfy the service demand with lowest operational cost, a BEB may be used to serve several trips consecutively during the daily operation period, and battery charging may be implemented between any two adjacent trips to ensure enough energy. For ease of elaboration, we refer to a series of trip services undergone by the same BEB during the daily operation period as *a trip chain* (Xu and Meng, 2019). To be specific, a trip chain r consists of a series of trips sorted in an ascending order in terms of their departure time, and can be expressed as:

$$r = (i_1, i_2, \cdots, i_{n_r}) \tag{2}$$

where n_r indicates the total number of trips covered in trip chain r.

The charging strategy along trip chain r with trips $i_1, i_2, \cdots, i_{n_r}$ is denoted as Ψ_r. It refers to the charging amount and specific charging moment between any two adjacent trips covered by the trip chain r; and can be expressed by:

$$\Psi_r = \left\{ \varphi_{i_k}, \mu_{i_k t} | k = 1, 2, \cdots, n_r - 1 \right\} \tag{3}$$

where φ_{i_k} is defined as a binary variable that equals 1 if charging operation is implemented between trips i_k and i_{k+1}, and 0 otherwise; $\mu_{i_k t}$ is also defined as a binary variable that equals 1 if BEB begins to charge in time step t after finishing trip i_k, and 0 otherwise. Due to limited charging facilities, if BEB begins to charge immediately on arrival, there may be no available charging facilities at present and the start time to be charged after each trip service should thus be optimized jointly. It is also worth to note that $\varphi_{i_{n_r}}$ is constant (i.e., $\varphi_{i_{n_r}} = 1$) because the charging operation is surely implemented at the end of each trip chain to prepare for the upcoming day's service. Meanwhile, we also pay less attention on the specific charge starting time after trip i_{n_r} as the BEB is out of service after that until the next day's service begins. Therefore, the charging strategy applied on BEB after trip i_{n_r} is ignored in Ψ_r, as the range of k shown in Eq. (3). In addition, the decision variable $\mu_{i_k t}$ should satisfy the following conditions:

$$\sum_{t \in T} \mu_{i_k t} = \varphi_{i_k}, \qquad \forall k = 1, 2, \cdots, n_r - 1 \tag{4a}$$

$$\sum_{t \in T} \mu_{i_k t} t + \left(1 - \varphi_{i_k}\right) M \geq s_{i_k} + e_{i_k}, \qquad \forall k = 1, 2, \cdots, n_r - 1 \tag{4b}$$

where M is a sufficiently large number. Constraint (4a) indicates that if the charging operation occurs after trip i_k (i.e., $\varphi_{i_k} = 1$), the charging operation must start in a certain time step, i.e., exists a time index t, such that $\mu_{i_k t}$ equals 1; otherwise, $\mu_{i_k t}$ equals 0 for all the time index $t \in T$. Constraint (4b) indicates that, if the charging operation occurs after trip i_k (i.e., $\varphi_{i_k} = 1$), then the starting time of charging operation (i.e., $\sum_{t \in T} \mu_{i_k t} t$) should be no earlier than the trip ending time (i.e., $s_{i_k} + e_{i_k}$).

A trip chain r with charging strategy Ψ_r is feasible, if the following conditions are fulfilled:

(1) all the covered trips can be performed on time;
(2) battery energy is sufficient to support all the covered trips given that BEB can be charged at terminal station if both time and charging facilities permit.

For trip chain r with trips $i_1, i_2, \cdots, i_{n_r}$, the first condition can be expressed by:

$$z_{i_k} \leq s_{i_{k+1}}, \qquad \forall k = 1, 2, \cdots, n_r - 1 \tag{5}$$

where z_{i_k} indicates the ready-to-depart time [time step] of BEB after finishing trip i_k. It equals the ending time of trip i_k if no charging operation occurs after trip i_k, i.e., trips i_k and i_{k+1} are covered seamlessly without charging operation; and equals the ending time of charging operation otherwise:

$$s_{i_k} + e_{i_k} - \varphi_{i_k} M \leq z_{i_k} \leq s_{i_k} + e_{i_k} + \varphi_{i_k} M, \qquad \forall k = 1, 2, \cdots, n_r - 1 \tag{6a}$$

$$\sum_{t \in T} \mu_{i_k t} t + g\left(SoC_{i_k}, SoC_{init}\right) - \left(1 - \varphi_{i_k}\right) M \leq z_{i_k} \leq \sum_{t \in T} \mu_{i_k t} t + g\left(SoC_{i_k}, SoC_{init}\right) + \left(1 - \varphi_{i_k}\right) M, \qquad \forall k = 1, 2, \cdots, n_r - 1 \tag{6b}$$

where SoC_{i_k} indicates the SoC at the end of trip i_k and $g\left(SoC_{i_k}, SoC_{init}\right)$ returns the number of time steps required to charge from SoC_{i_k} to SoC_{init}. In addition, the term $g\left(SoC_{i_k}, SoC_{init}\right)$ should align with the nonlinear charging profile of BEBs, which will be detailed in the following subsection.

For the trip chain r with trips $i_1, i_2, \cdots, i_{n_r}$, the SoC at the end of trip i_k, SoC_{i_k}, can be expressed recursively:

$$SoC_{i_k} = SoC_{init} - m_{i_k}, \text{if } k = 1 \tag{7a}$$

$$SoC_{i_{k-1}} - m_{i_k} - \varphi_{i_{k-1}} M \leq SoC_{i_k} \leq SoC_{i_{k-1}} - m_{i_k} + \varphi_{i_{k-1}} M, \qquad \forall k = 2, \cdots, n_r \tag{7b}$$

$$SoC_{init} - m_{i_k} - \left(1 - \varphi_{i_{k-1}}\right) M \leq SoC_{i_k} \leq SoC_{init} - m_{i_k} + \left(1 - \varphi_{i_{k-1}}\right) M, \qquad \forall k = 2, \cdots, n_r \tag{7c}$$

Constraint (7a) initializes the SoC of BEBs. Constraints (7b) and (7c) state that if BEB is replenished after trip i_{k-1}, the SoC of BEB is reset as SoC_{init} and SoC_{i_k} is equal to $SoC_{init} - m_{i_k}$; otherwise, SoC_{i_k} is equal to $SoC_{i_{k-1}} - m_{i_k}$.

Since the minimal SoC may occur at the end of each trip, the second condition to ensure feasibility of trip chain restricts that:

$$SoC_{i_k} \geq \underline{SoC}, \qquad \forall k = 1, 2, \cdots, n_r \tag{8}$$

where $\underline{SoC}$ denotes the lower bound of SoC to relax drivers from the range anxiety.

In light of the above, constraints (3)–(8) guarantee the feasibility of trip chain r with trips $i_1, i_2, \cdots, i_{n_r}$. Given trip chain r, the total operational cost along trip chain r, denoted as J_r, can be expressed as the sum of charging fees, $A(\Psi_r)$, cost incurred by battery degradation, $D(\Psi_r)$, and a fixed cost term related to bus acquisition (without battery), denoted by E and measured in \$/veh-day:

$$J_r = A(\Psi_r) + D(\Psi_r) + E \tag{9}$$

Here $A(\Psi_r)$ can be easily obtained via multiplying the total charging amount [kWh] by unit electricity price [\$/kWh], while the calculation of $D(\Psi_r)$ will be elaborated in the next subsection.

2.2. Modeling of battery aging mechanism

The capacity of lithium-ion batteries degrades during charging and discharging cycle, corresponding to cycle aging, thereby reducing the battery's available power output and shortening the vehicle's available range. To be specific, BEBs can be charged at the terminal station after trip service, while the discharge of the BEB battery occurs when the BEB travels on the road. Therefore, for BEB, the capacity fading resulting from cycle loss accumulates over the course of the whole trip chain taken by this BEB. Meanwhile, the capacity fading rate of lithium-ion batteries is highly related to SoCs in terms of both SoC variation and average SoC level: the higher either the SoC variation or average SoC level is, the faster battery capacity fades. Since different types of lithium-ion batteries present similar electrochemical properties as described above, without loss of generality, we assume that BEBs studied in this paper are equipped with a specific kind of lithium-ion batteries, i.e., LiFePO$_4$ cell. We borrow the empirical model developed by Lam and Bauer (2012) to describe the cycle aging of batteries over each charge and discharge cycle of LiFePO$_4$ cells. In particular, for trip chain r, if the
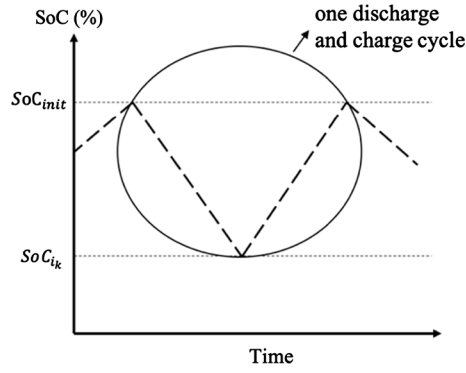
Fig. 3. Illustration of discharge and charge cycle.

(a) An example of trip chain
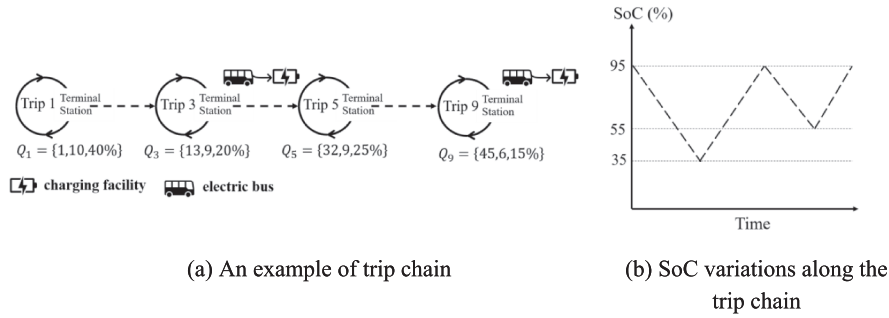
(b) SoC variations along the trip chain

Fig. 4. An example for BEB trip chain and corresponding SoC variations.

charging operation is implemented after finishing trip i_k, i.e. $\varphi_{i_k} = 1$, consider the cycle in terms of SoC decreasing from SoC_{init} to SoC_{i_k} and increasing back to SoC_{init} again, as illustrated in Fig. 3. This discharge and charge cycle is referred to Γ_{i_k} for short. It is worth to note that since the actual SoC variations along time during each cycle depend on the operation conditions of BEB as well as the battery charging profile, Fig. 3 is not to describe the exact SoC variations at the micro level, but to intuitively depict its change trend for the ease of presentation. The corresponding capacity fading rate occurring in cycle Γ_{i_k}, denoted as ξ, is expressed as a function of both SoC_{i_k} and SoC_{init}, as presented in Eq. (10a-c). It records the kWh faded per kWh processed during both charging and discharging operation. For example, if ξ equals 10^{-4}, it indicates that the battery capacity would fade by 10^{-4} kWh whenever 1 kWh is charged into the battery or discharged from the battery. A sketched derivation of Eq. (10a-c) is furnished in Appendix B in the interest of brevity.

$$\xi\left(SoC_{i_k}, SoC_{init}\right) = \gamma_1 SoC_{i_k, dev} \cdot e^{\gamma_2 SoC_{i_k, avg}} + \gamma_3 e^{\gamma_4 SoC_{i_k, dev}} \tag{10a}$$

where

$$SoC_{i_k, avg} = \frac{SoC_{init} + SoC_{i_k}}{2}, \tag{10b}$$

$$SoC_{i_k, dev} = \frac{SoC_{init} - SoC_{i_k}}{2} \tag{10c}$$

Here $SoC_{i_k, avg}$ records the average SoC in cycle Γ_{i_k}, while $SoC_{i_k, dev}$ captures the deviation of SoC from the average SoC value. Higher $SoC_{i_k, dev}$ corresponds to larger SoC variation, i.e. ΔSoC, where ΔSoC is defined as the difference between SoC_{init} and SoC_{i_k}. The coefficients $\gamma_1, \gamma_2, \gamma_3$ and γ_4 are constant model parameters.

In general, a BEB battery reaches EoL when its available capacity decreases to 70%-80% of its original capacity. This EoL related threshold is represented by χ. In this paper, χ equals 30%, indicating the battery reaches to its EoL when its current capacity declines by 30% of its initial capacity. When the battery reaches to EoL, it can be recycled for energy storage system. In our paper the salvage value of battery is set as W to represent its second-life application. Then for the discharge and charge cycle Γ_{i_k}, the corresponding cost incurred by battery degradation, denoted as $d\left(SoC_{i_k}, SoC_{init}\right)$, is thus calculated by:

$$d\left(SoC_{i_k}, SoC_{init}\right) = \frac{2 \times \xi\left(SoC_{i_k}, SoC_{init}\right) \times \left(SoC_{init} - SoC_{i_k}\right) \times \mathbb{Q}}{\chi \times \mathbb{Q}} (B - W)$$
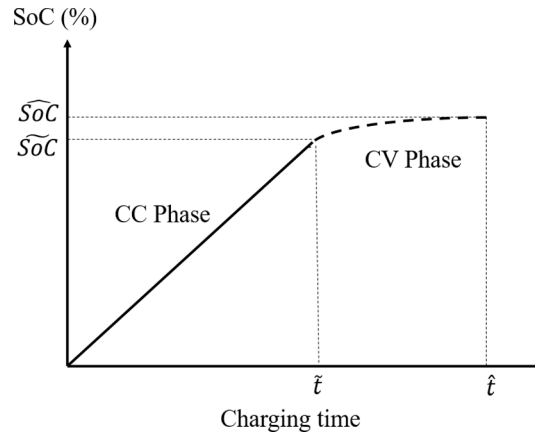
Fig. 5. Illustration of nonlinear charging profile.

$$= \frac{2 \times \xi\left(SoC_{i_k}, SoC_{init}\right) \times \left(SoC_{init} - SoC_{i_k}\right)}{\chi}(B - W) \tag{11}$$

where B indicates battery acquisition cost; $\mathbb{Q}$ denotes the battery capacity [kWh]. The term $2 \times \xi\left(SoC_{i_k}, SoC_{init}\right) \times \left(SoC_{init} - SoC_{i_k}\right) \times \mathbb{Q}$ is the faded capacity within cycle Γ_{i_k} [kWh]; and the term $\chi \times \mathbb{Q}$ represents the battery's effective capacity [kWh].

The total cost incurred by battery degradation in the course of trip chain r, $D(\Psi_r)$, is the sum of battery degradation cost occurring in each discharge and charge cycle:

$$D(\Psi_r) = \sum_{k=1}^{n_r-1} \varphi_{i_k} d\left(SoC_{i_k}, SoC_{init}\right) + d\left(SoC_{i_{n_r}}, SoC_{init}\right) \tag{12}$$

where the last term on the right-hand side of Eq. (12) is related to the charging operation implemented at the end of daily operation period. For the ease of presentation, we use the toy example presented in Fig. 4 to explain the cycle aging occurring over the trip chain. Here, it is supposed that we have 9 trips in the considered transit system and they are numbered by 1, 2, 3,···9 in an ascending order in terms of their departure time. Fig. 4 illustrates an example of BEB trip chain (i.e., trip 1→ trip 3→ trip 5→ trip 9) and its charging strategy (i.e., bus is charged between trip 3 and 5, and after trip 9), where SoC_{init} is set as 95% a priori. We can see that there are two discharge and charge cycles with SoC ranges as [35%, 95%] and [55%, 95%] respectively. These two cycles correspond to different battery capacity fading rates due to different lower bounds of SoC ranges. The related battery degradation cost along the trip chain example equals the sum of costs incurred by cycle loss occurring in these two cycles.

2.3. Nonlinear charging profile

The battery of BEB is generally charged with a constant current-constant voltage (CC-CV) or constant power-constant voltage (CP-CV) scheme (Liu, 2013). In both schemes, the battery's SoC concavely increases with respect to the charging time. As the proposed methodology is independent of the exact form of the charging profile, we assume without loss of generality that the BEBs are charged under CC-CV scheme, where the battery would undergo two phases, namely CC phase and CV phase. In the first phase (i.e., CC phase), the charging current is held constant and hence the SoC increases linearly with time until the battery's terminal voltage reaches the threshold. After that, the terminal voltage keeps constant (i.e., CV phase), thus resulting in the current decreasing exponentially and the SoC increasing concavely with respect to the charging time (Marra et al., 2012), as intuitively depicted in Fig. 5.

The battery nonlinear charging model with a CC-CV scheme can be presented by a piecewise function (Pelletier et al., 2017; Montoya et al., 2017). In particular, in the CC phase, the constant charging current is denoted by I_{cc}; then the SoC is a linear function of the charging time:

$$SoC(t) = \frac{\int I(t)dt}{\mathbb{A}} = \frac{I_{cc} \times t}{\mathbb{A}}, t \in \left[0, \tilde{t}\right] \tag{13}$$

where $\mathbb{A}$ indicates the battery capacity in the unit of Ah. After the SoC reaches the maximum achievable SoC in CC phase, denoted as $\widetilde{SoC}$, the SoC would increase slowly and enter into CV phase, which can be represented by a set of complex differential equations (Pelletier et al., 2017) or a piecewise linear function with gradually decreasing slopes (Montoya et al., 2017). This switch time point is denoted as $\tilde{t}$. For ease of presentation, the charging profile in CV phase is denoted as $\mathscr{F}(t)$:

$$SoC(t) = \mathscr{F}(t), t \in \left[\tilde{t}, \hat{t}\right] \tag{14}$$

As illustrated in Fig. 5, $\widehat{SoC}$ is the maximum value of SoC achievable at the end of CV phase and $\hat{t}$ indicates the time required to

charge to $\widetilde{SoC}$.

For trip chain r, if the charging operation is implemented after finishing trip i_k, i.e. $\varphi_{i_k} = 1$, the corresponding charging time $g_1\left(SoC_{i_k}, SoC_{init}\right)$ and number of required time steps $g\left(SoC_{i_k}, SoC_{init}\right)$ can be derived as:

$$
g_1\left(SoC_{i_k}, SoC_{init}\right) = \begin{cases} \dfrac{\left(SoC_{init} - SoC_{i_k}\right) \times \mathbb{A}}{I_{cc}}, & if \ \ SoC_{i_k} < SoC_{init} \leq \widetilde{SoC} \\[2ex] \mathscr{F}^{-1}(SoC_{init}) - \dfrac{SoC_{i_k} \times \mathbb{A}}{I_{cc}}, & if \ \ SoC_{i_k} \leq \widetilde{SoC} < SoC_{init} \\[2ex] \mathscr{F}^{-1}(SoC_{init}) - \mathscr{F}^{-1}\left(SoC_{i_k}\right), & if \ \ \widetilde{SoC} < SoC_{i_k} < SoC_{init} \end{cases}
\tag{15a}
$$

$$
g\left(SoC_{i_k}, SoC_{init}\right) = \left\lceil \frac{g_1\left(SoC_{i_k}, SoC_{init}\right)}{\mathscr{L}} \right\rceil
\tag{15b}
$$

where $\mathscr{F}^{-1}$ denotes the inverse function of $\mathscr{F}$; function $\lceil a \rceil$ returns the smallest integer that is no smaller than a.

2.4. Joint consideration of BEB service schedule, charging strategy and their impact on battery aging

To minimize the total operational cost, the charging strategy, i.e., charging amount/duration and the start time to be charged after each trip service, and its impact on battery aging should be jointly considered with the trip allocation plan. To the specific, the nonlinear charging profile indicates distinct charging efficiency when initiating charging at different SoC levels. It means that the charging amount does not increase linearly with charging time when $\widetilde{SoC} < SoC_{init}$, and the charging efficiency decreases as the initial charging SoC increases. However, if initiating charging with lower SoC, it may result in higher battery degradation cost due to larger SoC variations. In addition, the limited charging facilities entail the decision-makings more complicated, where the starting time to be charged should also be jointly optimized. If BEB begins to charge immediately on arrival, there may be no available charging facilities at present. However, if the BEB waits longer, it may miss the departure time of next trips.

As the battery degradation model and nonlinear charging profile have been nicely reflected in trip chains, the objective of this problem is to minimize the daily operational cost by finding the optimal trip chains from the pool of feasible trip chains to guarantee that the predefined trip set can be satisfied successfully while the capacity of charging facilities is not exceeded at each time step. Apparently, the proposed problem is NP-hard as its special case without the allowance of partial charging and ignoring battery degradation process has been demonstrated to be NP-hard (Rinaldi et al., 2019).

3. A set partitioning model

Let R denote the set of all feasible trip chains (i.e., including service sequence and charging strategy) within the daily operation period, satisfying the minimal battery level constraint. For each feasible trip chain $r \in R$, we define a binary variable λ_r, which equals one if and only if the trip chain r is selected; and to zero otherwise. Then the considered BEB scheduling problem can be formulated as a mixed integer linear programming, i.e., a set partitioning model:

Mathematical model [P1]

$$
\min J_{[P1]} = \sum_{r \in R} J_r \lambda_r
\tag{16a}
$$

subject to:

$$
\sum_{r \in R} H_i^r \lambda_r = 1, \quad \forall i \in I
\tag{16b}
$$

$$
\sum_{r \in R} U_t^r \lambda_r \leq C, \quad \forall t \in T
\tag{16c}
$$

$$
\lambda_r \in \{0, 1\}, \quad \forall r \in R
\tag{16d}
$$

Objective function (16a) minimizes the total operational cost within the daily operation period. Constraint (16b) ensures that each trip $i \in I$ is served exactly once in the solution, where coefficient H_i^r is set to one if trip i is covered in trip chain r and to zero otherwise. Constraint (16c) guarantees that the number of charging facilities used in each time step is no more than the limited capacity C; and U_t^r equals one if BEB is charged at time step t in trip chain r and to zero otherwise. Constraint (16d) defines the domains of decision variables $\lambda_r, r \in R$.

In the above objective function (16a), J_r denotes the operational cost of trip chain $r \in R$, including charging fees, cost incurred by battery degradation and the bus acquisition cost as shown in Eq. (9). Together with Eq. (9) and constraint (16b), we have:

$$
J_{[P1]} = \sum_{r \in R} J_r \lambda_r
$$

$$= \sum_{r\in R}A(\Psi_r)\lambda_r + \sum_{r\in R}D(\Psi_r)\lambda_r + \sum_{r\in R}\lambda_r E$$

$$= \varkappa\bullet\mathbb{Q}\bullet\sum_{i\in I}m_i + \sum_{r\in R}D(\Psi_r)\lambda_r + \sum_{r\in R}\lambda_r E \tag{17}$$

where $\varkappa$ indicates the unit electricity price [$/kWh]. It implies that the total charging fees is a constant term. Therefore, the charging fees are ignored in our model from now on.

The huge number of feasible trip chains (i.e., the number of decision variables) makes the model [P1] intractable even for a small size problem. It is thus time consuming to solve this problem directly via model [P1]. We next present a tailored B&P algorithm to solve this set partitioning model [P1].

4. Branch-and-price approach

The set partitioning model is a mixed integer linear programming and can be solved to optimality by B&P approach. Specifically, B&P is a combination of CG and B&B methods. In the B&P framework, the CG technique is adopted to solve the linear relaxation of this set partitioning model [P1], as shown in Section 4.1. Then, to guarantee the feasible integer solutions, a B&B scheme is used to obtain the optimal integer solution, as presented in Section 4.2. Section 4.3 presents the framework of B&P approach, where the efficiency of this tailored B&P approach highly depends on how to effectively solve the pricing problem by taking advantage of the unique problem features. That is the key and difficult part of the solution approach.

4.1. Column generation procedure

We now describe the CG procedure to solve linear relaxation of this set partitioning model, referred to as master problem (MP):
Mathematical model [P2]

$$\min J_{[P2]} = \sum_{r\in R}J_r\lambda_r \tag{18a}$$

subject to: (16b-c)

$$\lambda_r \geq 0 \tag{18d}$$

Here model [P2] contains all of the possible trip chains. Therefore, the size of R and the corresponding computational time grow exponentially with the problem size. To lower the dimension of model [P2], CG method is used to solve model [P2] by repeatedly solving (i) a restricted master problem (RMP) with a subset of trip chains (Section 4.1.1) and (ii) a pricing problem (Section 4.1.2) to generate new trip chains (i.e., columns) with negative reduced costs (for minimization problem). Column generation stabilization is presented in Section 4.1.3.

4.1.1. Restricted master problem of the column generation procedure
The RMP with a subset of feasible trip chains $R^{'} \in R$ is formulated in model [P3]. Initially, we derive $R^{'}$ by a heuristic algorithm to ensure the existence of a feasible initial solution in model [P3]. The details of heuristic algorithm to generate $R^{'}$ are relegated to Appendix C.
Mathematical model [P3]

$$\min J_{[P3]} = \sum_{r\in R^{'}}J_r\lambda_r \tag{19a}$$

subject to:

$$\sum_{r\in R^{'}}H_i^r\lambda_r = 1, \quad \forall i \in I \tag{19b}$$

$$\sum_{r\in R^{'}}U_t^r\lambda_r \leq C, \quad \forall t \in T \tag{19c}$$

$$\lambda_r \geq 0 \tag{19d}$$

The dual variables of model [P3] are defined as:
π_i: the dual variable for constraint (19b), $i \in I$;
β_t: the dual variable for constraint (19c), $t \in T$.
At each iteration of column generation, the dual variables of model [P3], $\Omega := \{\pi_i,\beta_t|i \in I, t \in T\}$ are the input parameters of pricing problem [P4] to generate new feasible trip chain (i.e., column) with the lowest reduced cost (i.e., the objective of model [P4]). The column generation procedure terminates when the minimal reduced cost is non-negative, indicating no feasible trip chains can be

added to R' in model [P3].

4.1.2. Pricing problem of the column generation procedure

To generate new columns, we next present the model of pricing problem. The goal of pricing problem is to find a feasible trip chain with negative reduced cost. In regard of this, the decision variables of pricing problem are defined as follows:

$\delta_{ij} \in \{0,1\}$: set to one if a BEB serves trips i and j consecutively, where trip i begins earlier than trip j (i.e., trip i immediately precedes trip j); and to zero otherwise, $i \in I \cup O. j \in I \cup D, i \neq j$; here, we use O and D simply to represent the original and destination depot respectively for notational convenience;

$\varphi_i \in \{0,1\}$: set to one if the charging operation is implemented after trip i and before serving the subsequent trip; and to zero otherwise, $i \in I$;

$\mu_{it} \in \{0,1\}$: set to one if BEB begins to charge in the time step t after trip i and before serving the subsequent trip; and to zero otherwise, $i \in I, t \in T$;

$\eta_{it} \in \{0,1\}$: set to one if BEB ends charging in the time step t after trip i and before serving the subsequent trip; and to zero otherwise, $i \in I, t \in T$;

$\phi_{it} \in \{0,1\}$: set to one if BEB is charged in the time step t after trip i and before serving the subsequent trip; and to zero otherwise, $i \in I, t \in T$.

According to the standard procedure of CG method, the model of pricing problem can be formulated as follows:

Mathematical model [P4]

$$\min J_{[P4]} = E + \sum_{i \in I} \varphi_i d(SoC_i, SoC_{init}) + \sum_{i \in I} \delta_{iD} d(SoC_i, SoC_{init}) - \sum_{i \in I} \pi_i \sum_{j \in I \cup D} \delta_{ij} - \sum_{t \in T} \sum_{i \in I} \phi_{it} \beta_t \tag{20a}$$

subject to:

$$\sum_{i \in I} \delta_{Oi} = 1 \tag{20b}$$

$$\sum_{i \in I} \delta_{iD} = 1 \tag{20c}$$

$$\sum_{j \in I \cup D} \delta_{ij} - \sum_{j \in I \cup O} \delta_{ji} = 0, \quad \forall i \in I \tag{20d}$$

$$\varphi_i \leq \sum_{j \in I} \delta_{ij}, \quad \forall i \in I \tag{20e}$$

$$\sum_{t \in T} \mu_{it} = \varphi_i, \quad \forall i \in I \tag{20f}$$

$$\sum_{t \in T} \eta_{it} = \varphi_i, \quad \forall i \in I \tag{20g}$$

$$\sum_{t \in T} \mu_{it} \cdot t + (1 - \varphi_i) M \geq s_i + e_i, \quad \forall i \in I \tag{20h}$$

$$\sum_{t \in T} \eta_{it} \cdot t \geq \sum_{t \in T} \mu_{it} \cdot t + g(SoC_i, SoC_{init}) - (1 - \varphi_i) M, \quad \forall i \in I \tag{20i}$$

$$\sum_{t \in T} \eta_{it} \cdot t \leq \sum_{t \in T} \mu_{it} \cdot t + g(SoC_i, SoC_{init}) + (1 - \varphi_i) M, \quad \forall i \in I \tag{20j}$$

$$\phi_{it} = \sum_{\tilde{t} \leq t} \mu_{i\tilde{t}} - \sum_{\tilde{t} \leq t} \eta_{i\tilde{t}}, \quad \forall i \in I, t \in T \tag{20k}$$

$$s_i + e_i \leq s_j + (1 - \delta_{ij}) M, \quad \forall i, j \in I \tag{20l}$$

$$\sum_{t \in T} \eta_{it} \cdot t \leq s_j + (1 - \delta_{ij}) M, \quad \forall i, j \in I \tag{20m}$$

$$SoC_i \leq SoC_{init} - m_i + (1 - \delta_{Oi}) M, \quad \forall i \in I \tag{20n}$$

$$SoC_i \geq SoC_{init} - m_i - (1 - \delta_{Oi}) M, \quad \forall i \in I \tag{20o}$$

$$SoC_j \leq SoC_i - m_j + (1 - \delta_{ij}) M + \varphi_i M, \quad \forall i, j \in I \tag{20p}$$
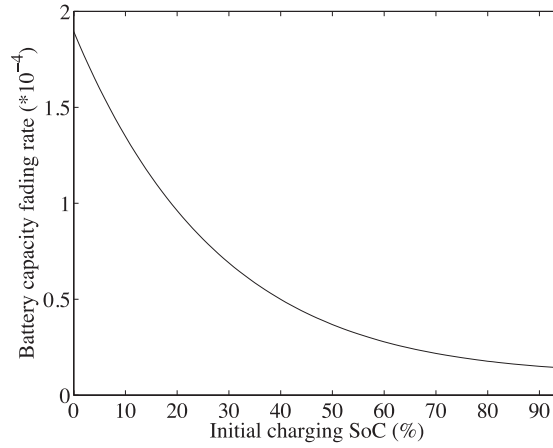
Fig. 6. Effect of initial charging SoC on battery degradation rate given $SoC_{init} = 95\%$.

$$SoC_j \geq SoC_i - m_j - (1 - \delta_{ij})M - \varphi_i M, \qquad \forall i, j \in I \tag{20q}$$

$$SoC_j \leq SoC_{init} - m_j + (1 - \delta_{ij})M + (1 - \varphi_i)M, \qquad \forall i, j \in I \tag{20r}$$

$$SoC_j \geq SoC_{init} - m_j - (1 - \delta_{ij})M - (1 - \varphi_i)M, \qquad \forall i, j \in I \tag{20s}$$

$$SoC_i \geq \underline{SoC}, \qquad \forall i \in I \tag{20t}$$

In the above model, the objective function (20a) is to minimize the reduced cost of BEB schedule, where the input parameters $\pi_i(i \in I)$ and $\beta_t(t \in T)$ are the dual variables of model [P3]. Constraints (20b-c) indicate a trip chain originates from depot O and terminates at depot D. Constraint (20d) represents covering and flow conservation. Constraint (20e) indicates that the charging operation may be implemented after a trip if the trip is covered by trip chain. Constraints (20f)–(20h) state that if charging operation is implemented, the charging operation must start and end in a certain time step, and the starting time should be no earlier than the trip ending time. Constraints (20i)–(20j) indicate that the ending time of charging operation is equal to the corresponding starting time plus required charging duration. Constraint (20k) links variable μ_{it}, η_{it} and φ_{it}. Constraints (20l)–(20m) ensure that the BEB must finish trip i or charging operation no later than the departure time of trip j if $\delta_{ij} = 1$. Constraints (20n)–(20o) indicate that the initial SoC of BEB is SoC_{init} when it departs from the original depot O. Constraints (20p)–(20s) capture the discharging/charging dynamics when δ_{ij} equals 1: if BEB is replenished after trip i, the SoC of BEB is reset as SoC_{init} and SoC_j is equal to $SoC_{init} - m_j$; otherwise, SoC_j is equal to $SoC_i - m_j$. Constraint (20t) guarantees that SoC should be no smaller than a predefined lower bound $\underline{SoC}$ to relax drivers from the range anxiety.

The pricing problem is an extension of resource constrained shortest path problem by allowing replenishment along a path. One of its special case is the resource constrained shortest path problem, which has been proved to be NP-hard (Garey and Johnson, 1979). Therefore, the pricing problem is also NP-hard. Meanwhile, the nonlinear charging profile makes the pricing problem nonlinear by nature; the complex expression of $d(SoC_i, SoC_{init})$ and limited charging facilities render the pricing problem more cumbersome to find the optimal solution by standard solution approach. Fortunately, we can take advantage of lithium-ion batteries' electrochemical properties to solve this pricing problem.

We firstly construct a pseudo-network denoted by $\mathbb{G} = (\mathbb{I} \cup O \cup D, \mathbb{L})$ to solve the pricing problem. Each trip $i \in I$ is represented by a node $i \in \mathbb{I}$ in the network. Meanwhile, node i is associated with node cost $-\pi_i$, electricity consumption m_i, departure time s_i and returning time $s_i + e_i$. All the nodes are sorted in ascending order in terms of the departure time and named in sequence as node 1, node 2, $\cdots$, until node $|I|$. The set of arcs $\mathbb{L}$ includes: (i) from original depot O to $i \in \mathbb{I}$; (ii) from $i \in \mathbb{I}$ to $j \in \mathbb{I}$ if $s_i + e_i \leq s_j$; and (iii) from $i \in \mathbb{I}$ to destination depot D. For each node $i \in \mathbb{I}$, it is associated with two charging operation choices: charging operation is implemented after trip i; or consecutively serve the upcoming trip without charging operation. The objective to find the trip chain with the minimal reduced cost is thus equivalent to finding the shortest path in the constructed network $\mathbb{G}$, where the arc distance/cost depends on the selected charging operation. Note that for node $i \in \mathbb{I}$, the number of required time steps for charging operation varies from its former connected nodes and selected charging operations. If the charging operation is implemented, we always choose the consecutive time steps with the lowest sum of $-\beta_t$ to finish each charging operation.

To reduce the searching space, the above constructed network should be preprocessed by eliminating the infeasible and un-optimal nodes and links. We firstly present an important electrochemical property of lithium-ion batteries, as detailed in the following lemma.

Lemma 1. *Given $SoC_{init} \in [70\%, 100\%]$, $\xi(SoC_0, SoC_{init})$ is a monotonically decreasing function of SoC_0.*

Lemma 1 can be proved by deriving $\frac{\partial \xi(SoC_0, SoC_{init})}{\partial SoC_0} < 0$. However, the derivation process is cumbersome due to the complex mathematical form of function $\xi(SoC_0, SoC_{init})$. Fortunately, SoC is recorded with the unit of 1% in practice. In regard of this, we could

approximate SoC as discrete variable, and Lemma 1 can thus be easily proved by comparing ξ under different SoC_0 values for a given $SoC_{init} \in [70\%, 100\%]$. For example, Fig. 6 intuitively presents the battery degradation rate along different initial charging SoCs (i.e., SoC_0), given $SoC_{init} = 95\%$. Lemma 1 indicates that the battery capacity fading rate is a monotonically increasing function of SoC variation ΔSoC, for a given $SoC_{init} \in [70\%, 100\%]$. Based upon Lemma 1, we next present Proposition 1 and Proposition 2 to build efficient solution approach for the pricing problem.

Proposition 1. *If the optimal value of model [P4], denoted as $J^*_{[P4]}$, is negative, there exists an optimal trip chain r^* such that for all the covered trips, we have $d(SoC_{init} - m_{i_k}, SoC_{init}) - \pi_{i_k} < 0, \forall k = 1, 2, \cdots, n_{r^*}$.*

Proof. We use contradiction to prove this proposition. The charging strategy along trip chain r^* is denoted as Ψ_{r^*}. Suppose there exists trip i_k covered in trip chain r^* such that $d(SoC_{init} - m_{i_k}, SoC_{init}) - \pi_{i_k} \geq 0$.

We next construct a new trip chain by removing trip i_k from trip chain r^*, denoted as $\tilde{r}$. The charging strategy in trip chain $\tilde{r}$, denoted as $\Psi_{\tilde{r}}$ is consistent with Ψ_{r^*}, except for the first charging operation implemented later than the ending of trip i_k. Without loss of generality, this charging operation is denoted as $\Psi^m_{r^*}$, the mth charging operation in Ψ_{r^*}, where the corresponding charging initial SoC and battery degradation rate are represented as $SoC^m_{r^*}$ and $\xi^m_{r^*}$, respectively.

Case 1. $SoC^m_{r^*} = SoC_{init} - m_{i_k}$

The replenished electricity is m_{i_k} in charging operation $\Psi^m_{r^*}$. Then we have:

$$\xi^m_{r^*} = \xi(SoC^m_{r^*}, SoC_{init})$$

$$= \xi(SoC_{init} - m_{i_k}, SoC_{init}) \tag{21}$$

In this scenario, the charging strategy $\Psi_{\tilde{r}}$ is obtained by removing m^{th} charging operation from Ψ_{r^*}. Therefore, the set of time steps occupied for charging operation in strategy $\Psi_{\tilde{r}}$ is a subset of that in strategy Ψ_{r^*}.

According to duality theory, we have:

$$\beta_t \leq 0, \qquad \forall t \in T \tag{22}$$

Consequently, the cost term related to $-\sum_{t \in T}\sum_{i \in I}\phi_{it}\beta_t$ in strategy Ψ_{r^*}, denoted as $-\sum_{t \in T}\sum_{i \in I}\phi_{it}\beta_t|\Psi_{r^*}$ for short, is no smaller than that in $\Psi_{\tilde{r}}$, denoted as $-\sum_{t \in T}\sum_{i \in I}\phi_{it}\beta_t|\Psi_{\tilde{r}}$:

$$-\sum_{t \in T}\sum_{i \in I}\phi_{it}\beta_t|\Psi_{r^*} \geq -\sum_{t \in T}\sum_{i \in I}\phi_{it}\beta_t|\Psi_{\tilde{r}} \tag{23}$$

Then compare the reduced cost of trip chain r^* and $\tilde{r}$, we have:

$$J_{[P4]}(r^*, \Psi_{r^*}) - J_{[P4]}(\tilde{r}, \Psi_{\tilde{r}})$$

$$= d(SoC_{init} - m_{i_k}, SoC_{init}) - \pi_{i_k} - \sum_{t \in T}\sum_{i \in I}\phi_{it}\beta_t|\Psi_{r^*} + \sum_{t \in T}\sum_{i \in I}\phi_{it}\beta_t|\Psi_{\tilde{r}}$$

$$\geq d(SoC_{init} - m_{i_k}, SoC_{init}) - \pi_{i_k}$$

$$\geq 0 \tag{24}$$

Hence,

$$J_{[P4]}(r^*, \Psi_{r^*}) \geq J_{[P4]}(\tilde{r}, \Psi_{\tilde{r}}) \tag{25}$$

The above inequality is strict if there exists at least one time step t, such that:

(i) $\beta_t < 0$;
(ii) BEB is charged in time step t in the mth charging operation of strategy Ψ_{r^*}

Therefore, we can conclude that Proposition 1 holds on in case 1.

Case 2. $SoC^m_{r^*} < SoC_{init} - m_{i_k}$

The replenished electricity is larger than m_{i_k} in charging operation $\Psi^m_{r^*}$. According to Lemma 1, we have:

$$\xi^m_{r^*} = \xi(SoC^m_{r^*}, SoC_{init}) > \xi(SoC^m_{r^*} + m_{i_k}, SoC_{init}) \tag{26}$$

and

$$\xi^m_{r^*} = \xi(SoC^m_{r^*}, SoC_{init}) > \xi(SoC_{init} - m_{i_k}, SoC_{init}) \tag{27}$$

Compared with Ψ_{r^*}, the charging duration of mth charging operation is shortened in the rebuilt charging strategy $\Psi_{\tilde{r}}$, because trip i_k is removed and less electricity is replenished. Similarly, we have:

$$-\sum_{t\in T}\sum_{i\in I}\phi_{it}\beta_t|\Psi_{r^*} \geq -\sum_{t\in T}\sum_{i\in I}\phi_{it}\beta_t|\Psi_{\widetilde{r}} \tag{28}$$

Then compare the reduced cost of trip chain r^* and $\widetilde{r}$, the following in equation holds on:

$$J_{[P4]}(r^*,\Psi_{r^*}) - J_{[P4]}(\widetilde{r},\Psi_{\widetilde{r}})$$

$$= d(SoC_{r^*}^m, SoC_{init}) - d(SoC_{r^*}^m + m_{i_k}, SoC_{init}) - \pi_{i_k} - \sum_{t\in T}\sum_{i\in I}\phi_{it}\beta_t|\Psi_{r^*} + \sum_{t\in T}\sum_{i\in I}\phi_{it}\beta_t|\Psi_{\widetilde{r}}$$

$$= 2\xi(SoC_{r^*}^m, SoC_{init})\bullet(SoC_{init} - SoC_{r^*}^m)\bullet(B-W)\Big/\chi - 2\xi(SoC_{r^*}^m + m_{i_k}, SoC_{init})\bullet(SoC_{init} - SoC_{r^*}^m - m_{i_{n_k}})\bullet(B-W)\Big/\chi - \pi_{i_k}$$

$$\quad - \sum_{t\in T}\sum_{i\in I}\phi_{it}\beta_t|\Psi_{r^*} + \sum_{t\in T}\sum_{i\in I}\phi_{it}\beta_t|\Psi_{\widetilde{r}}$$

$$> 2\xi(SoC_{r^*}^m, SoC_{init})m_{i_k}\bullet(B-W)\Big/\chi - \pi_{i_k}$$

$$> 2\xi(SoC_{init} - m_{i_k}, SoC_{init})m_{i_k}\bullet(B-W)\Big/\chi - \pi_{i_k}$$

$$= d(SoC_{init} - m_{i_k}, SoC_{init}) - \pi_{i_k}$$

$$\geq 0 \tag{29}$$

Hence,

$$J_{[P4]}(r^*,\Psi_{r^*}) > J_{[P4]}(\widetilde{r},\Psi_{\widetilde{r}}) \tag{30}$$

Eq. (30) indicates that trip chain r^* is not the optimal solution of pricing problem; i.e., trip i_k should not be covered at optimality. Hence, Proposition 1 also holds on in case 2. ∎

Proposition 1 implies that any node $i \in \mathbb{I}$ with node cost satisfying $d(SoC_{init} - m_i, SoC_{init}) - \pi_i \geq 0$, could be excluded from the constructed network $\mathbb{G}$, and the corresponding links are removed accordingly. Furthermore, if $d(SoC_{init} - m_i, SoC_{init}) - \pi_i \geq 0$ for all $i \in I$, we have $J_{[P4]}^* \geq 0$ and the column generation procedure terminates.

Upon the preprocessed network described above, we then design a label correcting algorithm by fully considering the unique features of pricing problem. The replenishment opportunities entail multiple labels at each node in the network. Specifically, a label at a node $i \in \mathbb{I}$ represents a partial path p_i from the original depot O to the node i, and is measured by a two-dimensional vector: (the reduced cost of the path, final SoC of the path), denoted as $(a(p_i), S(p_i))$. Path p_i records the decision-makings in terms of trip service sequence and corresponding charging strategy from the original depot O to the node i. Upon path p_i, we can always construct the subsequent path from node i to destination depot D, and their combination forms a complete path from the original depot O to destination depot D, denoted as $\overline{p_i}$.

To reduce the number of node labels and improve computational efficiency, we can readily present the dominance rule detailed in the following proposition, by making use of the monotonicity of battery aging function indicated in Lemma 1. Note that, the integration of battery capacity fading mechanism and nonlinear charging profile distinguishes the pricing problem studied in our paper from traditional shortest path problem. Therefore, it should be further verified whether the widely-adopted multi-label correcting algorithm is still applicable for the pricing problem studied in our paper, including the design of multiple labels as well as the dominance rule, as what we will present in Proposition 2.

Proposition 2. *Give two partial paths from the original depot O to node i, $p_{i,1}$ and $p_{i,2}$, the labels of node i along paths $p_{i,1}$ and $p_{i,2}$ are $\left(a(p_{i,1}), S(p_{i,1})\right)$ and $\left(a(p_{i,2}), S(p_{i,2})\right)$ respectively. Label $\left(a(p_{i,1}), S(p_{i,1})\right)$ dominates $\left(a(p_{i,2}), S(p_{i,2})\right)$, if both of the following conditions are satisfied:*

$$a(p_{i,1}) \leq a(p_{i,2}) \tag{31a}$$

$$S(p_{i,1}) \geq S(p_{i,2}) \tag{31b}$$

and at least one of above inequalities is strict.

Proof. We will demonstrate that for any complete path $\overline{p_{i,2}}$ built upon $p_{i,2}$, we can always construct a complete path $\overline{p_{i,1}}$ built upon $p_{i,1}$, such that:

$$a(\overline{p_{i,1}}) < a(\overline{p_{i,2}}) \tag{32}$$

Case 1. $S(p_{i,1}) = S(p_{i,2})$
Then we have

$$a(p_{i,1}) < a(p_{i,2}) \tag{33}$$

In this scenario, given any complete path $\overline{p_{i,2}}$, $\overline{p_{i,1}}$ is built as follows:

In $\overline{p_{i,1}}$, the subsequent covered trips and applied charging strategy after trip i are exactly same as that in $\overline{p_{i,2}}$. Obviously, the following inequality holds:

$$a(\overline{p_{i,1}}) - a(\overline{p_{i,2}})$$

$$= a(p_{i,1}) - a(p_{i,2})$$

$$< 0 \tag{34}$$

Case 2. $S(p_{i,1}) > S(p_{i,2})$

In this scenario, given any complete path $\overline{p_{i,2}}$, $\overline{p_{i,1}}$ is built as follows:

In $\overline{p_{i,1}}$, the subsequent covered trips and charge starting time after trip i are exactly same as that in $\overline{p_{i,2}}$. However, the inequality $S(p_{i,1}) > S(p_{i,2})$ indicates that in path $\overline{p_{i,1}}$, the initial charging SoC of the first charging operation implemented after trip i is higher than that in path $\overline{p_{i,2}}$, which results in shorter charging duration and lower cost incurred by battery degradation (see Lemma 1). Therefore, we can conclude that inequation (32) still holds in case 2. ∎

According to the dominance rule implied in Proposition 2, a label no longer needs to be extended whenever it is dominated by another label. In the proposed multi-label correcting method, each node i is assumed to be associated with multiple labels which represent a partial path ending at trip i. At node i, label k is represented as $l_k(i) := [\gamma_k, \kappa_k, a_k, S_k]$, where γ_k and κ_k are the node and label index that preceded label k and would be used to identify the traversed nodes of that path by back-tracking. Then label $l_{k_1}(i)$ dominates $l_{k_2}(i)$ if (1) $a_{k_1} \leq a_{k_2}$; and (2) $S_{k_1} \geq S_{k_2}$, where at least one of above inequalities is strict. Meanwhile, S_k would also be used to identify the charging operation choice implemented before trip i by back-tracking: if $S_k = SoC_{init} - m_i$, charging operation occurs between node/trip i and its preceded node; otherwise, node i and its preceded node are covered seamlessly without charging operation.

Suppose we have a non-dominated label k at node i, represented as $l_k(i) = [\gamma_k, \kappa_k, a_k, S_k]$, and there exists a link from node i to node j. Then extended from label $l_k(i)$, the following labels are generated at node j, depending on the charging operation choice:

(1) Charging operation is not implemented between trip i and j, i.e., $\varphi_i = 0$:

If the energy is sufficient to support trip j, i.e., $S_k - m_j \geq \underline{SoC}$, then a label $l_{u_1}(j) = [i, k, a_k - \pi_j, S_k - m_j]$ will be generated at node j;

(2) Charging operation is implemented between trip i and j, i.e., $\varphi_i = 1$:

If time permits, i.e., $s_j - s_i - e_i \geq g(S_k, SoC_{init})$, then a label $l_{u_2}(j) = [i, k, a_k - \pi_j + d(S_k, SoC_{init}) - \sum_{t \in T} \phi_{it} \beta_t, SoC_{init} - m_j]$ will be generated at node j.

The above-mentioned label dominance and extension rule are placed into a framework of the general label-correcting algorithm to solve the pricing problem. Although the multi-label method works in a label correcting way, the ascending ordering of trips guarantees the generated labels are permanent even in a network with negative node cost. This feature greatly reduces the unnecessary label updating, and thus significantly improves the computational efficiency of the proposed label correcting method. It is also worth to note that, the proposed label dominance rule is only viable for the monotonicity of battery degradation function and analogous property still holds for other types of lithium-ion batteries, instead of being limited to LiFePO$_4$ cells. Therefore, the proposed method is also applicable for the scheduling of BEBs equipped with other types of lithium-ion batteries.

4.1.3. Column generation stabilization

A major difficulty in column generation may be the slow convergence when the solution is near the optimum, which is called the tailing-off effect. To mitigate this effect, we use a dual stabilization approach (Addis et al., 2012; Wang et al., 2018). Initially, we set $\overline{\Omega} := \left\{ \overline{\pi}_i, \overline{\beta}_t | i \in I, t \in T \right\}$ as vector **0**. At each iteration of the column generation procedure, we obtain a dual vector by solving model [P3], denoted as $\Omega := \{ \pi_i, \beta_t | i \in I, t \in T \}$; then we use a modified dual vector $\widetilde{\Omega}$ as input parameters for the pricing subproblem [P4]:

$$\widetilde{\Omega} = \rho \bullet \Omega + (1 - \rho) \bullet \overline{\Omega}, \rho \in [0, 1] \tag{35}$$

For a given ρ (set as 0.6 initially in this paper), the column procedure is executed until no columns can be added to model [P3]. Then we update $\overline{\Omega} \leftarrow \widetilde{\Omega}$, and increase ρ (by 0.1 in this paper) for a new iteration of the above process. The column procedure terminates when $\rho = 1$ and no columns can be added.

Meanwhile, our preliminary experiments show that selecting multiple trip chains with negative reduced cost when solving pricing problem is helpful for speeding up the column generation procedure in BEB scheduling. Therefore, to accelerate the column generation process, we add several columns to the RMP in each iteration. To be specific, at destination depot, all the labels $l_k(D)$ satisfying $a_k < 0$ are preserved and the corresponding trip chains are all added to $R^{'}$ in model [P3].

4.2. Branching strategy and upper bounding

Since the solution to the MP may not be integer, a B&B procedure is necessary to obtain optimal integer solutions. An intuitive approach is to branch on the variable λ_r. However, it would result in an imbalanced search tree. Therefore, we develop another branching strategy.

If an optimal solution to the MP is not integer, then there must exist a pair of trips $i, j \in I$ such that $0 < \sum_{r \in R} \delta_{ij} \lambda_r < 1$ (Desrochers and Soumis, 1989). Then branching is applied on a fractional $\sum_{r \in R} \delta_{ij} \lambda_r$, where we always select the largest fractional $\sum_{r \in R} \delta_{ij} \lambda_r$ to branch. The underlying network is changed according to $\sum_{r \in R} \delta_{ij} \lambda_r = 1$ or $\sum_{r \in R} \delta_{ij} \lambda_r = 0$. For each pair of trips that should be excluded, we will delete the corresponding link in the network, while for each pair of trips that should be included, we will retain the corresponding link and delete all the other links originating from the tail of the corresponding link or heading to the head of the corresponding link. To obtain a feasible solution quickly, we select the node with minimum lower bound (*LB*) in node list. Meanwhile, when selecting a node on the same level, we always select the node with $\sum_{r \in R} \delta_{ij} \lambda_r = 1$. We can also pre-specify a relative optimality tolerance level ε, $0 < \varepsilon < 1$, for controlling the gap associated with branching. If the incumbent best upper bound on model [P1] is *UB* (i.e., the objective value of model [P1] for the best integer solution obtained) and the optimal objective value of MP in a branch is not smaller than $UB/(1 + \varepsilon)$, then the branch can be pruned. The B&P approach provides an ε-optimal solution.

To reduce the tree size of B&B search, we also develop a heuristic algorithm based on the CG procedure to generate good upper bounding. In the proposed heuristic algorithm, the inner procedure is the CG procedure described in Section 4.1; the outer procedure is the selection strategies used to obtain an integer solution.

Firstly, we modify constraint (16c) in model [P1] as:

$$\sum_{r \in R} U_t^r \lambda_r \leq C_t, \quad \forall t \in T \tag{36}$$

Initially, C_t is constant and equal to C. Then the available number of charging facilities at each time step may decrease as the outer procedure proceeds in our heuristic algorithm. To be specific, every time the inner CG procedure stops, we select the feasible trip with the largest value of the decision variables λ_r. Then update C_t and I for a new iteration of the above process:

(i) if BEB is charged in time step t according to the selected trip chain, update $C_t \leftarrow C_t - 1$;
(ii) if trip i is covered in the selected trip chain, update $I \leftarrow I \backslash \{i\}$;

The algorithm terminates when all the trips are covered.

4.3. Framework of a branch-and-price algorithm

In this section, we illustrate the framework of the B&P algorithm as follows. This framework combines the CG procedure and a B&B tree.

Step 0: Define the relative optimality tolerance of branching as ε. Clear the current node list of the B&B tree; set the RMP with the initial set of feasible trip chains as the current parent node; and set *UB* as the corresponding optimal objective value and x^* as the optimal solution. The *UB* is used to record the incumbent best objective value and the x^* is used to record the incumbent best feasible solution.

Step 1: Solve MP of current parent node by CG. The solution and the objective of MP of current parent node are denoted by x and $LpObj(x)$, respectively.

    Step 1.1: if x is an integer solution and $LpObj(x) < UB$, update $UB \leftarrow LpObj(x), x^* \leftarrow x$, prune this node, and go to step 3; if x is an integer solution and $LpObj(x) \geq UB$, prune this node, and go to step 3;

    Step 1.2: if x is not an integer solution and $LpObj(x) < UB/(1 + \varepsilon)$, update UB using the heuristic algorithm presented in Section 4.2 and go to step 2; if x is not an integer solution and $LpObj(x) \geq UB/(1 + \varepsilon)$, prune this node, and go to step 3.

Step 2: Choose the branching variable and branch the current parent node into two child nodes (i.e., a left child node and a right child node) as described in Section 4.2. (the left child node ensures $\sum_{r \in R} \delta_{ij} \lambda_r = 1$, while the right child node ensures $\sum_{r \in R} \delta_{ij} \lambda_r = 0$); activate the left child node as the new current parent node; add the right child node into the current node list and set its *LB* with the value of $LpObj(x)$; then, go to step 1.

Step 3: Mark all the nodes in current node list, satisfying that the node's *LB* is no smaller than $UB/(1 + \varepsilon)$, as inactive and remove them from the current node list. If the current node list is empty, stop the whole algorithm; otherwise, activate the node in the current node list with the lowest *LB* and set this node as the current parent node. Afterward, go to step 1.

5. Performance of the solution approach

Section 5.1 presents the parameter values used in numerical experiments. Section 5.2 evaluates the computational efficiency of our proposed solution approach. All the numerical instances in this paper are carried out via Matlab R2018b on an HP 2.11 GHz personal computer with 16 GB RAM.

Table 1
Parameter definitions and values.

Parameter	Notation	Value	Unit
Lower bound of battery level	$\underline{SoC}$	20	%
Unit acquisition cost of a BEB (without battery) per day	E	16.5	$
Battery capacity	$\mathbb{Q}$	162	kWh
Battery acquisition cost	B	28,000	$
Salvage value of battery	W	2,800	$
EoL related threshold	χ	0.2	–
Coefficient for battery degradation model	γ_1	−4.09e-4	–
Coefficient for battery degradation model	γ_2	−2.167	–
Coefficient for battery degradation model	γ_3	1.418e-5	–
Coefficient for battery degradation model	γ_4	6.13	–
Maximum achievable SoC in CC phase	$\widetilde{SoC}$	80	%
Maximum achievable SoC in CV phase	$\widehat{SoC}$	100	%
Time required to charge to $\widetilde{SoC}$	$\widetilde{t}$	2	hour
Time required to charge to $\widehat{SoC}$	$\widehat{t}$	3	hour
Optimality tolerance	ε	0.01	–

Table 2
Scale of instance groups.

Instance batch	Duration of daily operation (hr)	Unit of time step (min)	No. of time steps	No. of trips	No. of charging facilities
INB1	10	10	60	60	3
INB2	12	10	72	80	5
INB3	12	5	144	80	6
INB4	12	5	144	120	8
INB5	14	5	168	160	10

Table 3
Cost and runtimes of our proposed B&P solution approach.

| Instance		Obj ($)	Fleet size	T_CPU Time (s)	PP_CPU Time (s)	PP/T_CPU Time	#PP	PP_CPU Time/#PP (s)	#Node
Batch	ID								
INB1	1	594.2	23	104	11	11%	183	0.06	2
	2	599.1	23	102	11	11%	185	0.06	2
	3	637.0	25	106	11	10%	182	0.06	3
	4	586.9	24	95	9	9%	187	0.05	2
	5	589.4	23	106	11	10%	190	0.06	2
INB2	6	713.6	30	224	54	24%	464	0.12	4
	7	744.1	29	291	72	25%	575	0.13	5
	8	709.6	27	204	45	22%	436	0.10	4
	9	696.7	28	363	87	24%	747	0.12	6
	10	762.1	31	257	64	25%	462	0.14	4
INB3	11	715.6	30	268	67	25%	502	0.13	4
	12	730.3	30	268	61	23%	428	0.14	5
	13	678.5	28	301	65	22%	414	0.16	5
	14	727.7	30	249	49	20%	442	0.11	4
	15	704.7	30	393	96	24%	709	0.14	6
INB4	16	1099.6	44	2503	722	29%	1676	0.43	6
	17	1168.3	47	2292	648	28%	1656	0.39	6
	18	1102.7	44	2188	693	32%	1881	0.37	9
	19	1046.6	42	2454	709	29%	1660	0.43	8
	20	1054.9	42	2566	766	30%	1579	0.49	7
INB5	21	1148.4	47	6874	2475	37%	2526	0.98	10
	22	1126.8	46	6120	2264	37%	2695	0.84	9
	23	1287.9	49	7733	3171	41%	3109	1.02	8
	24	1257.1	49	8340	3253	39%	3128	1.04	10
	25	1304.8	49	7562	2798	37%	2945	0.95	7
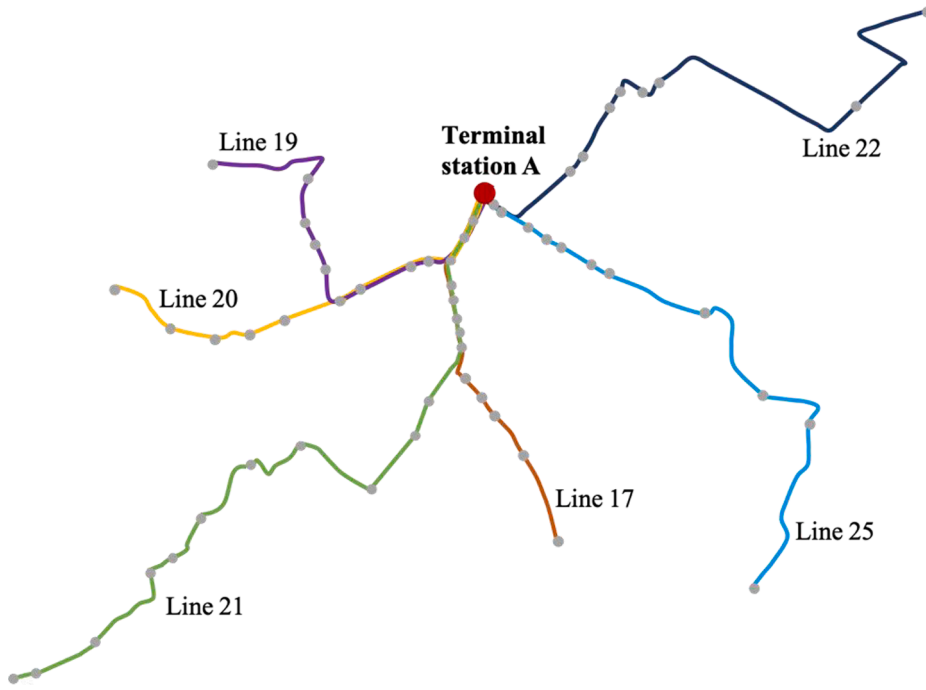
Fig. 7. Geographical distribution of selected bus lines departing from terminal station A.

5.1. Parameter values

The technical parameters needed for this paper are obtained from Yutong ZK6850BEVG53 used in a number of cities in China, given in Table 1. Yutong ZK6850BEVG53 is a kind of medium BEB, with vehicle length as 8.5 m. The parameter values for battery capacity fading model ($\gamma_1, \gamma_2, \gamma_3$ and γ_4) are borrowed from Lam and Bauer (2012). The charging profile in CV phase $\mathscr{F}(t)$ is approximated by a piecewise linear function under normal charging mode (Montoya et al., 2017):

$$SoC(t) = \begin{cases} 0.4t & t \in [0,2) \\ 0.8 + 0.25(t-2) & t \in [2, 2.2) \\ 0.85 + 0.1875(t - 2.2) & t \in [2.2, 3] \end{cases} \tag{37}$$

Note that the proposed solution method is only viable for monotonicity of battery degradation function with regards to the SoC variations and is independent of exact mathematical form of battery charging profile. Our method is thus also applicable for the scenario where nonlinear charging profile is represented by a set of differential equations (Pelletier et al., 2017), and the same to the CP-CV nonlinear charging profile.

5.2. Performance of branch-and-price solution approach

In the computation experiments, we tested 5 batches of numerical instances with different scales as listed in Table 2. In order to generate the random instances, the departure time of each trip is an integer randomly chosen from interval [1, total number of time steps]. The travel distance of each trip is randomly chosen from the set $\{20, 25, 30, 35, 40, 45\}$ km. Given an average travel speed $v = 17.5$ km/hr, the travel duration of each trip is thus calculated as $\left\lceil \frac{travel\_distance}{v\mathscr{L}} \right\rceil$, where the units of time step $\mathscr{L}$ for each batch of numerical instances are summarized in Table 2. The energy consumption rate is assumed to be 1.35 kWh/km (Gao et al., 2017). The value of SoC_{init} is randomly selected from the set $\{75\%, 80\%, 85\%, 95\%, 100\%\}$.

The solution quality and computational time of the 5 batches of numerical instances are presented in Table 3; and each batch includes 5 instances with randomly generated trip starting time and travel duration. The relative optimality tolerance of branching ε is set as 0.01. As presented in Table 3, column 1 and 2 provide the problem instance; each row corresponds to the results obtained for the corresponding instance. Columns 3–10 present the computational results of the proposed B&P solution approach from several aspects, including the objective value of model [P1] (Obj), the optimal BEB fleet size, the CPU time to obtain the optimal solution (T_CPU Time), the total CPU time spend on solving pricing problem (PP_CPU Time), the ratio of PP_CPU time to T_CPU time (PP/T_CPU Time), the running times of pricing problem (#PP), the unit time for solving pricing problem (PP_CPU Time/#PP) and the number of nodes traversed (#Node). It is worth mentioning that the columns can be generated from two sources in our paper: multiple columns generated in each run of the pricing problem and construction of initial solution pools. Therefore, we present the running times of

Table 4
Timetables for selected bus lines, departing from terminal station A.

| Line 17	Line 19	Line 20	Line 21	Line 22	Line 25
07:00:00	06:10:00	07:00:00	06:20:00	06:30:00	06:40:00
07:20:00	Every 20 min	07:30:00	Every 30 min	Every 30 min	07:10:00
07:40:00	09:10:00	08:00:00	18:50:00	17:30:00	07:40:00
Every 15 min	Every 30 min	Every 15 min			Every 20 min
10:40:00	15:10:00	14:15:00			18:20:00
Every 30 min	Every 20 min	14:45:00			18:50:00
16:40:00	19:10:00	15:15:00			19:20:00
Every 15 min		Every 15 min			19:50:00
19:25:00		20:30:00			
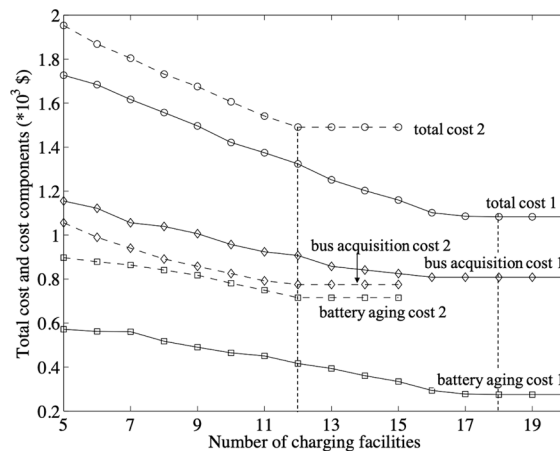
Fig. 8. Effects of the number of charging facilities on the optimal costs (1: considering battery aging; 2: without considering battery aging).

pricing problem, instead of the number of generated columns, and the former one would be much less than the latter.

According to the total CPU time in the table, we can see that, on average, the B&P approach can solve the media-size problems to optimality within 2.4 h. We also find that, the computational efficiency is largely and negatively affected by the number of trips, while it is less dependent on the number of time steps (compare the total CPU time of INB 2 and INB 3). Closer investigation of the solution processes unveils that the percentage of CPU time spent on solving pricing problem also increases as the size of problem grows, and the percentage is up to 41% in some cases, which also indicates that the efficiency of the B&P approach largely depends on the computational efficiency of CG, i.e., the multi-label correcting method for pricing problem. The ratio of CPU time spent on pricing problem to the running times of pricing problem reflects the computational efficiency of the proposed multi-label correcting method. It can be seen that both the running times of pricing problem and the average computational time on each run of pricing problem increase apparently with the growing number of trips. It is worth to note that, the network preprocessing and dominance rule, as unveiled in Proposition 1 and Proposition 2, play a vital role in speeding up the computational efficiency of CG procedure. To confirm the above claim, we further tested numerous instants without using these techniques (i.e., as benchmark for comparisons), and found that the computational efficiency without these techniques is consistently much slower than that with these techniques; and the computational advantage increases as the problem size grows. For scale instance INB5, the benchmark approach could not converge within 24 h, while our approach still could find the optimal solution within acceptable runtimes (less than 2.4 h), see the fifth column in Table 3. The details are omitted for brevity. Thanks to this advantage, the proposed method can be used to solve larger-scale problems with more service routes, and with a finer decision-making time scale (e.g., 5 min or less) within only moderate runtimes.

6. Numerical case studies

To validate our model, in this section we focus on a real-life case study arising from a major city in China. We consider a major bus terminal within the city, denoted as terminal station A. Departing from terminal station A, six yet-to-be-electrified lines are studied, namely line 17, 19, 20, 21, 22 and 25, as presented in Fig. 7. These six lines exhibit considerably high heterogeneity, in terms of both lengths and travel duration. To be specific, the lengths of the six lines are 11 km, 11.5 km, 12.6 km, 19.3 km, 16 km and 16.8 km respectively. Their travel durations (terminal to terminal) are 80 min, 90 min, 105 min, 150 min, 120 min and 130 min respectively.
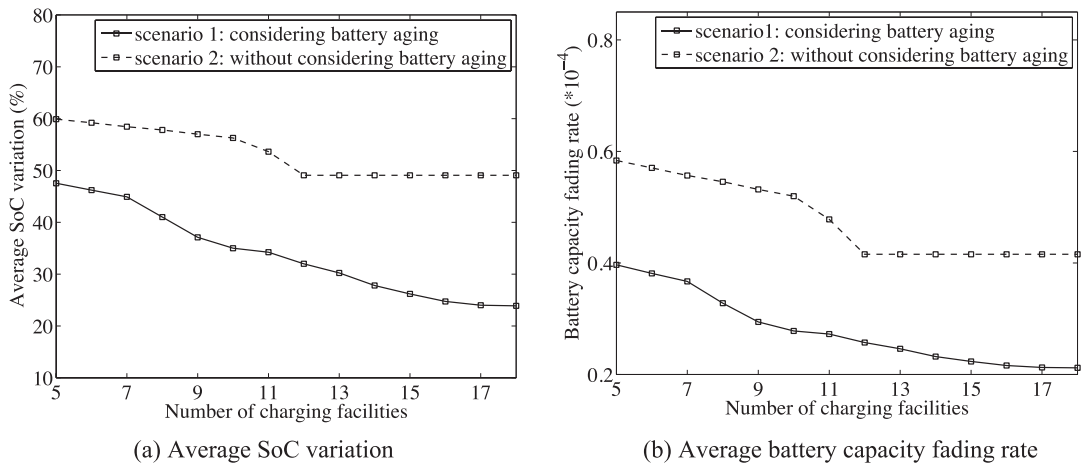
(a) Average SoC variation

(b) Average battery capacity fading rate

Fig. 9. Effects of the number of charging facilities on charging strategy.

(a) Considering battery aging
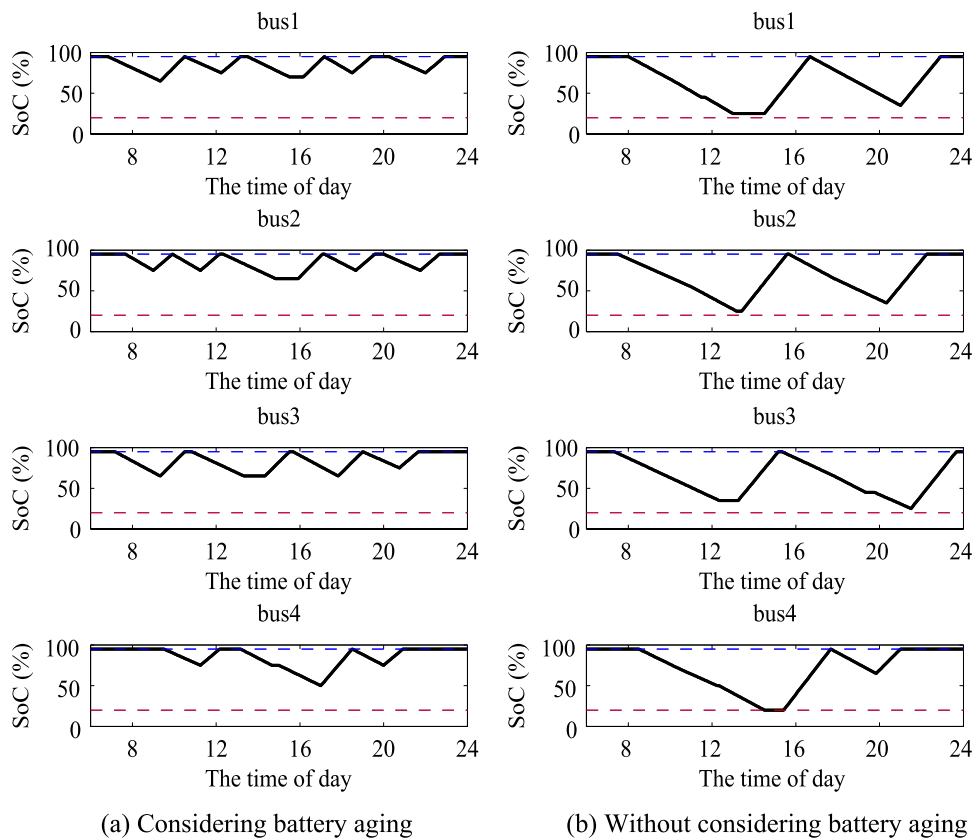
(b) Without considering battery aging

Fig. 10. SoC distribution of selected BEBs.

The timetables for these six lines are shown in Table 4. We use the piecewise linear charging function specified in Section 5.1, and the parameter values specified in Table 1 to conduct the following numerical cases. In this section, the relative optimality tolerance of branching ε is set as 0.05 for the purpose of computation efficiency.

First, we optimize the BEB service and charging schedule under a range of charging station capacity: $C \in [5, 20]$, where SoC_{init} is set as 95%. The optimal total operational cost and the cost components are plotted against C as the solid curve presented in Fig. 8. The figure shows that the optimal total cost (the solid curve with circle markers, named total cost 1) decreases as C increases, until it
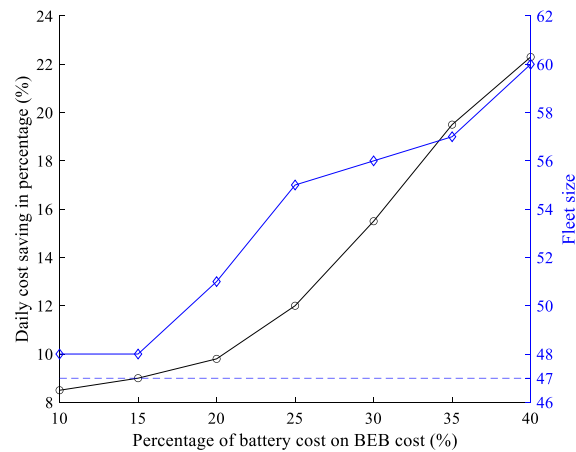
Fig. 11. Daily cost saving and optimal fleet size under various cost structures.

reaches a threshold of 18, as marked by the vertical dashed curve on the right-hand side of Fig. 8. This threshold represents the maximum number of charging facilities needed for BEBs at terminal station A; i.e., any additional charging facilities would be redundant, and the optimal total cost would stay the same ($1.083 × 10³).

The figure also shows that the cost incurred by bus acquisition (the diamond-marked solid curve, denoted as bus acquisition cost 1 for short) also decreases as C increases, which is expected. When more charging facilities are available, the waiting time of BEBs for charging at terminal station would reduce and the charging opportunity increases. Therefore, less BEBs are required to finish the predefined trip service. Meanwhile, the cost incurred by battery degradation (the square-marked solid curve, denoted as battery aging cost 1) also diminishes as C increases. This is because the SoC variation negatively affects battery aging rate: the larger the SoC variation is, the faster the battery degrades. Hence, when the charging facilities are relatively sufficient, the BEBs tend to be charged *as frequently as possible*, to achieve more cost saving by extending batteries' lifespan.

To examine the significance of taking battery health into consideration in BEB scheduling optimization framework, we also compare the above total cost and cost components against those for BEB scheduling without considering the cost incurred by battery aging, which is defined as scenario 2 from now on and plotted as the dashed curves in Fig. 8. Comparison reveals a total cost saving of 10.1–27.3% from battery management for $C \in [5, 20]$. If battery degradation is ignored in the optimization model, the major constraint for BEB scheduling lies in the limited charging facilities. The nonlinear charging profile indicates distinct charging efficiency when initiating charging at different SoC levels. To be specific, the deeper the depth of battery discharge is (i.e., larger SoC variation), the higher the charging efficiency is. Therefore, when the number of charging facilities is limited, BEB would be charged *as late as possible*. This charging strategy entails smaller fleet size of BEBs (the diamond-marked dashed curve, denoted as bus acquisition cost 2), while it accelerates the battery aging process and results in higher cost incurred by battery capacity fading (the square-marked dashed curve, denoted as battery aging cost 2). Specifically, battery aging cost is reduced by 35.1–61.6% by incorporating battery health considerations into the optimization framework of BEB scheduling.

The average SoC variation under each scenario and the corresponding battery capacity fading rate are plotted in Fig. 9a and b respectively. Here, we use the battery capacity fading rate corresponding to the average SoC variation to predict the battery's lifespan approximately. In both scenarios, the average SoC variation decreases as the number of charging facilities increases, and the same to the corresponding battery capacity fading rate. Further comparison between these two scenarios reveals that the average SoC variation is decreased by 20.6–51.3% for $C \in [5, 18]$ from battery health considerations. The average battery fading rate in scenario 1 is only 51.1–67.9% of that in scenario 2, indicating that the battery's service life can be extended by additional 47.2–96.1% approximately. This comparison further verifies the significance of battery management in BEB scheduling.

The difference of average SoC variations in the above two scenarios is further explained by Fig. 10, where the SoC curve of individual BEB against the time of day under each scenario is plotted. Due to limited space, we only present the SoC curves of four selected BEBs from the BEB fleet, where the capacity of charging facilities is set as 12, and SoC_{init} equals 95%. The blue dashed curve at the top of each figure indicates the value of SoC_{init}, while the red dashed curve at the bottom of each figure represents the predefined minimal SoC value (i.e., $\underline{SoC}$) to relax drivers from the range anxiety. Fig. 10 unveils considerable differences in terms of charging frequency and cycling SoC swing under two scenarios, which is consistent with the findings obtained from Figs. 8 and 9. In addition, we also find that, due to limited charging facilities, BEBs usually wait for a while before the charging operation.

Upon the above discussions, the operators are recommended to buy a few additional BEBs so that the lifespan of batteries can be extended by constraining the SoC within a narrow range and the total operational cost of BEB fleet can be saved to some extent. It is worth to note that, this finding is highly related to the proportion of battery packs' cost relative to BEBs' cost, instead of the absolute
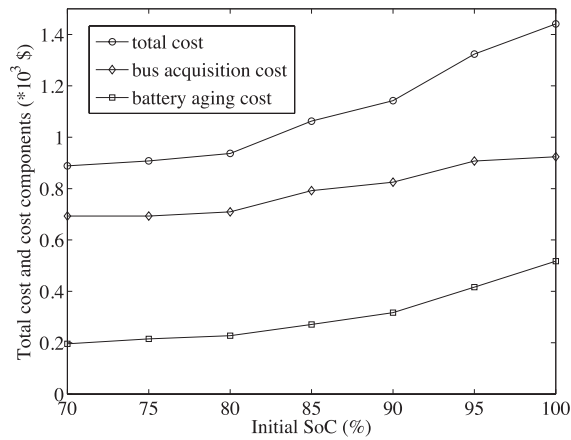
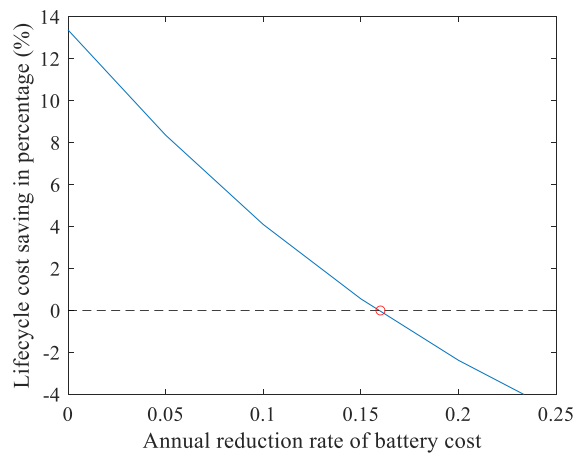**Fig. 12.** Effects of *SoC_init* on the optimal costs.

Fig. D1. Lifecycle cost saving under various annual reduction rates of battery cost.
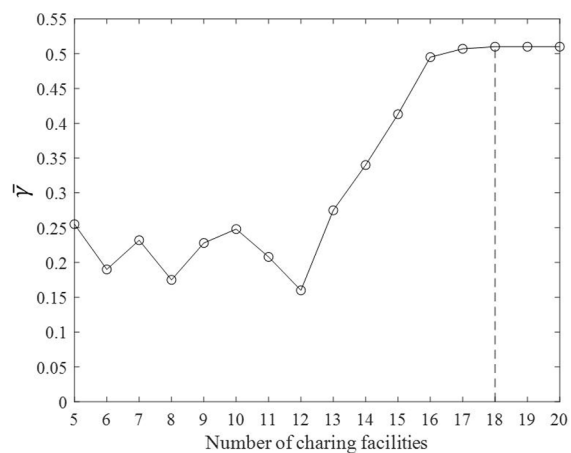

Fig. D2. Effect of the number of charging facilities on the threshold value $\bar{\gamma}$.

price of either battery packs or BEBs (in our paper, the percentage equals 27.9%). However, the percentage of battery cost may vary from case to case, depending on the type of studied BEB instances. Therefore, we further study the daily cost saving as well as fleet size under various cost structures. To this end, we gradually improve the unit acquisition cost of bus (without battery) per day, *E*, and keep

other parameters unchanged, so that the percentage of battery cost decreases progressively; and re-examine the cost saving and the optimal fleet size. The results are summarized in Fig. 11, where the number of charging facilities is set as 12 and SoC_{init} equals 95%. As expected, the benefit brought by battery management becomes less significant (the circle-marked solid curve) as the percentage of battery cost declines. However, a total cost saving of over 8.5% can still be achieved even if the percentage declines to 10%. Further investigation unveils that, as the proportion of battery-related cost declines, the optimal fleet size also decreases gradually (the diamond-marked solid curve), until it closely approaches to or equals the fleet size where battery aging is ignored in the optimization framework (the dashed curve at the bottom of the figure). It indicates that if the battery-related cost component takes only a small proportion of the total, the operators prefer to buy less additional buses and replace batteries more frequently due to their relatively low acquisition cost.

Besides cost stuctures, the declining trend in battery cost is another important concern. As revealed in our paper, the lifespan of batteries is prolonged at the cost of more BEBs involved. Meanwhile, we also note that with the development of technology, the price of battery packs has been descending gradually over the past years and will continuously come down in the future. Thus, battery management problem seems to be a less-important concern as compared to the fleet size issue from the long-term perspective. However, that is not the case. Actually, incorporating battery management into BEB scheduling can bring a certain number of cost saving from both short-term and long-term perspective, even though the price of battery packs is expected to decline in the near future. An idealized model is introduced to manifest that and the details are relegated to Appendix D for brevity.

Last, we investigate the optimal costs under various initial SoCs, $SoC_{init} \in [70\%, 100\%]$. The optimal cost and cost components are plotted in Fig. 12, where the number of charging facilities is set as 12. The figure shows that the total cost and all the cost components increase as the SoC_{init} grows. The cost incurred by battery degradation increases as the battery capacity fading rate is negatively affected by average SoC level. Larger SoC_{init} indicates higher average SoC level, thereby speeding up the battery degradation and resulting in the growth of battery aging cost. Meanwhile, to compete against this negative effect, the SoC range would be further narrowed, which causes a larger fleet size, i.e., the bus acquisition cost gradually grows as SoC_{init} increases. In addition, the increasing trend of BEB fleet size is also a natural result of nonlinear charging profile. To be specific, the charging efficiency keeps constant when $SoC_{init} \leq \widetilde{SoC}$ (here $\widetilde{SoC}$ is equal to 80%). However, when $SoC_{init} > \widetilde{SoC}$, the charging efficiency decreases as SoC_{init} increases. Therefore, the fleet size keeps constant at beginning and then gradually grows as the SoC_{init} increases to 100%.

7. Conclusions

In this study, we investigate the optimal service and charge strategy of BEB fleet, by taking battery degradation and nonlinear charging profile into account. Based on the set partitioning model, a B&P approach was developed to find optimal solution. By making use of the electrochemical properties of batteries in BEBs, a multi-label correcting method is proposed to solve the essential pricing problem. The efficiency and applicability of the proposed solution method were evaluated by extensive numerical experiments with randomly generated instances and real case studies. Our work has extended the literature in the realm of BEB scheduling in multiple aspects. We are, to our best knowledge, the first to formulate and solve BEB scheduling problem that incorporates battery degradation mechanism into optimization framework. The inclusion of battery health considerations makes the decision-makings more complicated. Despite the added complexity, the media-sized problem can still be solved within reasonable runtimes, thanks to the multi-label correcting method used to solve the pricing problem. Note that, since all types of lithium-ion batteries embedded in BEBs exhibit similar electrochemical properties, the proposed solution method is also applicable for the scheduling of BEBs equipped with other kinds of lithium-ion batteries, instead of being limited to $LiFePO_4$ battery cells. Meanwhile, our numerical case studies reveal a number of useful findings and the general findings hold on for BEBs charged under both CC-CV and CP-CV schemes. For example, the operators are encouraged to keep the initial SoC at a low level to achieve more cost saving. The results also show that by incorporating battery health considerations into BEB scheduling framework, the optimal total cost can be saved up to 10.1–27.3% and the battery's service life can be extended by additional 47.2-96.1% approximately.

In the future work, we would make more efforts to further improve our work, including relaxing the assumption of fixed initial SoC, considering multiple charging mode (e.g., fast charging and battery swapping) and extending the current single-terminal transit network to the multi-terminal one. Works in the above directions are under investigation now.

CRediT authorship contribution statement

Le Zhang: Conceptualization, Writing – original draft. **Shuaian Wang:** Supervision, Writing – review & editing. **Xiaobo Qu:** Conceptualization, Methodology, Validation, Resources, Supervision, Writing – review & editing.

Declaration of Competing Interest

The authors declare that they have no known competing financial interests or personal relationships that could have appeared to influence the work reported in this paper.

Acknowledgement

Appendix A. List of notations

Notation	Description
Indices	
i, j	bus round-trips;
t	time steps;
r	trip chains;
Decision variables	
$\delta_{ij} \in \{0,1\}$	set to one if an BEB serves trips i and j consecutively, where trip i begins earlier than trip j (i.e., trip i immediately precedes trip j); and to zero otherwise, $i \in I \cup O, j \in I \cup D, i \neq j$
$\mu_{it} \in \{0,1\}$	set to one if BEB begins to charge in the time step t after trip i and before serving the subsequent trip; and to zero otherwise, $i \in I, t \in T$;
$\varphi_i \in \{0,1\}$	set to one if the charging operation is implemented after trip i and before serving the subsequent trip; and to zero otherwise, $i \in I, t \in T$;
$\phi_{it} \in \{0,1\}$	set to one if BEB is charged in the time step t after trip i and before serving the subsequent trip; and to zero otherwise, $i \in I, t \in T$;
$\eta_{it} \in \{0,1\}$	set to one if BEB ends charging in the time step t after trip i and before serving the subsequent trip; and to zero otherwise, $i \in I, t \in T$;
$\lambda_r \in \{0,1\}$	set to one if trip chain r is selected; and zero otherwise, $r \in R$
Parameters and other variables	
I	set of trips;
T	set of time steps;
R	set of all feasible trip chains;
$R^{\grave{}}$	subset of R;
J	total operational cost
J_r	total operational cost along trip chain $r, r \in R$
s_i	departure time of trip $i, i \in I$;
e_i	travel time of trip $i, i \in I$;
C	capacity of charging station;
$\underline{SoC}$	minimal SoC value to reduce range anxiety;
m_i	proportion of electricity consumed with respect to the maximum possible charge it can hold in trip $i, i \in I$;
SoC_{init}	initial SoC of BEB at the very beginning of daily operation period;
SoC_i	SoC right at the end of trip $i, i \in I$;
$g_1(SoC_i, SoC_{init})$	time required to charge from SoC_i to SoC_{init};
$g(SoC_i, SoC_{init})$	number of time steps required to charge from SoC_i to SoC_{init};
z_i	ready-to-departure time of BEB after finishing trip $i, i \in I$;
M	sufficiently large number;
E	a fixed cost term related to bus acquisition;
Ψ_r	charging strategy of trip chain $r, r \in R$;
$D(\Psi_r)$	battery degradation cost occurred in charging strategy Ψ_r;
$A(\Psi_r)$	battery charging fee occurred in charging strategy Ψ_r;
ξ	battery capacity fading rate
B	unit battery acquisition cost;
χ	EoL-related threshold;
W	salvage value of battery;
H_i^r	set to one if trip i is covered in trip chain r; and to zero otherwise, $i \in I, r \in R$;
U_t^r	set to one if bus is charged at time step t in trip chain r; and to zero otherwise, $t \in T, r \in R$;
π_i	dual variables for constraint (19b), $i \in I$;
β_t	dual variables for constraint (19c), $t \in T$;
$\mathscr{T}(t)$	charging profile in CV phase;
$\mathscr{T}^{-1}$	inverse function of $\mathscr{T}$;
I_{cc}	constant charging current;
$\mathscr{L}$	length of unit time;
$S(p_i)$	final SoC of path p_i
$a(p_i)$	reduced cost of path p_i
$\mathbb{A}$	battery capacity in the unit of Ah;
$\mathbb{Q}$	battery capacity in the unit of kWh;
$\varkappa$	unit electricity price
$\widehat{SoC}$	maximum value of SoC achievable at the end of CV phase;
$\widetilde{SoC}$	maximum value of SoC achievable in CC phase;
$\widehat{t}$	time required to charge to $\widehat{SoC}$;
$\widetilde{t}$	time required to charge to $\widetilde{SoC}$;
$P_{\ddot{t}, bat}$	number of batteries purchased at time $\ddot{t}$
$P_{\ddot{t}, bus}$	number of BEBs without batteries purchased at time $\ddot{t}$
$A_{\ddot{t}, bat}$	purchase cost of batteries at time $\ddot{t}$
$A_{\ddot{t}, bus}$	purchase cost of BEBs without batteries at time $\ddot{t}$
$S_{\ddot{t}, bat}{}^{\ddot{T}}$	salvage value of batteries at the end of planning horizon
$S_{\ddot{t}, bus}{}^{\ddot{T}}$	salvage value of BEBs without batteries at the end of planning horizon
$\ddot{T}$	planning horizon

(*continued*)

Notation	Description
ϖ	reduction rate of battery cost
$C_{\ddot{T},\ddot{t}}$	capacity of batteries purchased at time $\ddot{t}$, at the end of planning horizon
$\bar{\gamma}$	threshold value
r	discount rate

Appendix B. Derivation of Eq. (10a-c)

In Lam and Bauer (2012), the capacity fading rate is calculated as follows:

$$\xi\left(SoC_{i_k}, SoC_{init}\right) = \gamma_1 SoC_{i_k,dev} \cdot e^{\gamma_2 SoC_{i_k,avg}} + \gamma_3 e^{\gamma_4 SoC_{i_k,dev}} \tag{B1}$$

where

$$SoC_{i_k,avg} = \frac{1}{\Delta Ah} \int_{Ah_{i_k,0}}^{Ah_{i_k}} SoC(Ah)dAh \tag{B2}$$

$$SoC_{i_k,dev} = \sqrt{\frac{3}{\Delta Ah} \int_{Ah_{i_k,0}}^{Ah_{i_k}} \left(SoC(Ah) - SoC_{i_k,avg}\right)^2 dAh} \tag{B3}$$

where $Ah_{i_k,0}$ is the initial amount of charged Ah before the $SoC_{i_k,avg}$ determination, Ah_{i_k} is the final amount of charged Ah in the charging period $g(SoC_{i_k}, SoC_{init})$, and ΔAh equals $Ah_{i_k} - Ah_{i_k,0}$. $SoC(Ah)$ represents the relationship between SoC and the processed Ah. Without loss of generality, SoC is assumed to be linearly increasing with the processed Ah (Lu et al., 2013):

$$SoC = f(Ah) = \frac{Ah}{\mathbb{A}} \tag{B4}$$

where $\mathbb{A}$ indicates the battery capacity in the unit of Ah. In the field of battery cells, the battery capacity, discharge and charge process can be described in the unit of either kWh or Ah. They are equivalent under rated voltage. Then $SoC_{i_k,avg}$ and $SoC_{i_k,dev}$ can be expressed as a function of SoC_{init} and SoC_{i_k}:

$$SoC_{i_k,avg} = \frac{1}{SoC_{init}\mathbb{A} - SoC_{i_k}\mathbb{A}} \int_{SoC_{i_k}\mathbb{A}}^{SoC_{init}\mathbb{A}} \frac{Ah}{\mathbb{A}} dAh$$

$$= \frac{SoC_{init} + SoC_{i_k}}{2} \tag{B5}$$

$$SoC_{i_k,dev} = \sqrt{\frac{3}{SoC_{init}\mathbb{A} - SoC_{i_k}\mathbb{A}} \int_{SoC_{i_k}\mathbb{A}}^{SoC_{init}\mathbb{A}} \left(\frac{Ah}{\mathbb{A}} - SoC_{i_k,avg}\right)^2 dAh}$$

$$= \sqrt{\frac{\left(SoC_{init} - SoC_{i_k,avg}\right)^3 - \left(SoC_{i_k} - SoC_{i_k,avg}\right)^3}{SoC_{init} - SoC_{i_k}}}$$

$$= \frac{SoC_{init} - SoC_{i_k}}{2} \tag{B6}$$

Appendix C. Heuristic algorithm to generate initial trip chain set $R^{'}$

The heuristic algorithm follows this logic: at beginning, the initial SoC of BEB is SoC_{init} when it departs from original depot O. Then the BEB will serve for the trip with the earliest departure time by now, denoted as i. After the BEB returns, check if the BEB could still serve for another trip satisfying the minimal battery level constraint or not. If so, choose the trip with the earliest departure time, denoted as j. Otherwise, choose available time steps (i.e., there exist available charging facilities) and charge bus until the battery level reaches to SoC_{init}. If still no trips can be served, connect the current trip to depot D, and save this trip chain in set $R^{'}$. The algorithm is detailed as follows.

Algorithm C1. (*Pseudocode to generate initial trip chain set R'*)

```
1   Initialize R' = ∅;
2   Sort the trips in set I in an ascending order in terms of their departure time;
3   Do:
4      i = I(1); %I(1) denotes the trip in set I with the earliest departure time
5      Initialize S = (i) (i.e, δ_Oi = 1), SoC = SoC_init − m_i, ready-to-go = s_i + e_i;
6      I ← I\{i}; %exclude trip i from setI
7      Do:
8         Find the set of trips 𝕁_1, satisfying (i) s_j ≥ ready-to-go; (ii) SoC − m_j ≥ SoC;
9         Find the set of trips 𝕁_2, satisfying s_j ≥ ready-to-go;
10        If 𝕁_1 ≠ ∅
11           Select the trip with the earliest stating time in 𝕁_1, denoted as j;
12           S ← (S, j), i.e., δ_ij = 1; %trip j will be served after tripi
13           I ← I\{j}; SoC ← SoC − m_j; i ← j;
14           ready-to-go = s_j + e_j;
15        ElseIf 𝕁_2 == ∅
16           S ← (S, D) (i.e., δ_iD = 1); R' ← {R', S}; j ← D;
17           Update the number of available charging facilities at each time step;
18        Else
19           SoC ← SoC_init;
20           Find g(SoC, SoC_init) continuous available time steps after trip i;
21           Update ready-to-go;
22        End If
23     Untilj == D
24  Until I == ∅.
```

Appendix D. An idealized model to manifest the significance of battery management from the life-cycle perspective

In the idealized model, we borrow the insights unveiled in Section 6 directly. To be specific, for the real-life case study conducted in Section 6, when the number of charging facilities installed at terminal station is 12: the optimal fleet size is 55 (see Fig. 8) and the average SoC variation of BEBs is 32% (see Fig. 9(a)) (named as fleet 1 from now on), if battery aging is jointly considered in the optimization framework; otherwise, the optimal fleet size and the corresponding average SoC variation are 47 and 49.7% respectively (named as fleet 2 from now on). It is assumed that BEBs are charged whenever its SoC variation reaches to the average one in each scenario.

We next study whether battery management is still a cost-efficient choice or not in the long term, given that the price of battery packs is certain to fall down over the following years. To this end, we compare the lifecycle cost of these two fleets (i.e., fleet 1 and fleet 2) over a relatively long planning horizon $\ddot{T}$, including the purchase costs of batteries and vehicles (i.e., BEBs without batteries), and their salvage values, as presented in Eq. (D1). Here, batteries and vehicles are considered separately due to their different lifespans. The batteries installed on the BEBs will be replaced by the new ones if they reach to EoL, and the same to the vehicles. When either the battery or vehicle reaches to EoL, its salvage value is set as 0 for simplicity (i.e., ignoring their second-life application). Therefore, we only concern their salvage values at the end of planning horizon, as shown in Eq. (D1). Since the salvage value is usually a minor part as compared to the purchase cost, this idealization would not affect the value of findings revealed in the following paragraphs.

$$J = \sum_{\ddot{t}=1}^{\ddot{T}} P_{\ddot{t},bus} A_{\ddot{t},bus} e^{-r\ddot{t}} + \sum_{\ddot{t}=1}^{\ddot{T}} P_{\ddot{t},bat} A_{\ddot{t},bat} e^{-r\ddot{t}} - \sum_{\ddot{t}=1}^{\ddot{T}} P_{\ddot{t},bus} S_{\ddot{t},bus}^{\ddot{T}} e^{-r\ddot{T}} - \sum_{\ddot{t}=1}^{\ddot{T}} P_{\ddot{t},bat} S_{\ddot{t},bat}^{\ddot{T}} e^{-r\ddot{T}} \tag{D1}$$

where $\ddot{t}$ is the time index; $P_{\ddot{t},bat}$ and $P_{\ddot{t},bus}$ indicate the number of batteries and vehicles purchased at time $\ddot{t}$ respectively; $A_{\ddot{t},bat}$ and $A_{\ddot{t},bus}$ represent the purchase cost of batteries and BEBs without batteries at time $\ddot{t}$ respectively; and $S_{\ddot{t},bat}^{\ddot{T}}$ and $S_{\ddot{t},bus}^{\ddot{T}}$ denote their corresponding salvage values at the end of planning horizon, which are purchased at time $\ddot{t}$; and r is the discount rate. Here, r is set as 0.07/12, with the time unit as one month. Also note that, the operation cost of BEB fleet is ignored in the calculation of lifecycle cost, as the operation cost, depended on service demand, keeps same for the two fleets.

In the idealized model, the battery cost is assumed to fall down exponentially with respect to the time:

$$A_{\ddot{t},bat} = (1 - \varpi)^{(\ddot{t}-1)/12} A_{1,bat} \quad \forall 2 \leq \ddot{t} \leq \ddot{T} \tag{D2}$$

$$0 < \varpi < 1 \tag{D3}$$

where ϖ denotes the annual reduction rate of battery cost. It is worth to note that, if the battery cost function is defined in other mathematical forms, e.g., a linear function of time, similar insights unveiled in the following paragraphs sill hold on.

The salvage value of a battery is defined as a function of its current capacity:

$$S_{\ddot{t},bat}^{\ddot{T}} = \max\left\{0, A_{\ddot{t},bat}\left(C_{\ddot{T},\ddot{t}} - \beta\mathbb{Q}\right)\Big/(\chi\mathbb{Q})\right\} \tag{D4}$$

where $C_{\ddot{T},\ddot{t}}$ denotes at the end of planning horizon $\ddot{T}$, the capacity of batteries purchased at time $\ddot{t}$; and β equals $1 - \chi$. When the battery reaches to EoL, its salvage value is set as 0; otherwise, it is set to be the initial battery acquisition cost multiplied by the percentage of remaining effective capacity, where the term $\chi\mathbb{Q}$ indicates effective battery capacity, and $C_{\ddot{T},\ddot{t}} - \beta\mathbb{Q}$ denotes the remaining effective capacity. The battery capacity is updated according to its cumulative utilization, where the total daily demand of BEB fleet in the unit of kilometer keeps consistent with that in Section 6; see Table 4. Meanwhile, the average battery energy consumption per kilometer [kWh/km] is 1.35 kWh/km, borrowed from Gao et al. (2017). The battery degradation mechanism and the corresponding parameter values are given in Section 2.2 and Section 5.1, respectively. Since the reference service life of vehicles is 12 years (Lajunen, 2018), we also set the planning horizon as 12 years for simplicity (i.e., $\ddot{T} = 144$). Then, at the end of planning horizon, the salvage value of BEBs without batteries (term $\sum_{\ddot{t}=1}^{\ddot{T}} P_{\ddot{t},bus} S_{\ddot{t},bus} \ddot{T} e^{-r\ddot{T}}$) can be omitted.

The lifecycle cost savings against annual reduction rate ϖ are plotted in Fig. D1, where the lifecycle cost saving in percentage is defined as:

$$\frac{[\text{lifecycle cost of fleet } \textit{without} \text{ considering battery aging}] - [\text{lifecycle cost of fleet } \textit{with} \text{ considering battery aging}]}{[\text{lifecycle cost of fleet } \textit{without} \text{ considering battery aging}]}$$

A positive cost saving indicates that incorporating battery management into BEB scheduling problem can result in a total cost saving over the given planning horizon. The figure shows that the percentage of lifecycle cost saving decreases as the annual reduction rate ϖ increases, which is expected. Theoretically, the faster the cost of battery packs declines, the more cost can be saved by purchasing batteries as late as possible, which can offset against the benefit brought by battery management to some extent. It is worth to note that the cost saving keeps positive until the annual reduction rate ϖ reaches to a threshold of 0.16, as marked by the red circle marker and denoted as $\bar{\gamma}$ from now on. When ϖ is smaller than the threshold value, a certain number of cost saving (up to 13.4%) can be achieved by involving battery management into fleet size decision problem from the life-cycle perspective. However, the lifecycle cost of fleet *with* considering battery aging would exceed that *without* considering battery aging, if the annual reduction rate ϖ is larger than the threshold value $\bar{\gamma}$.

We next study the effect of the number of charging facilities on the threshold value $\bar{\gamma}$, as presented in Fig. D2. When the number of charging facilities increases from 5 to 12, $\bar{\gamma}$ fluctuates within a small range [0.16, 0.25]. After that, the threshold value gradually grows as the number of charging facilities increases, until the number of charging facilities reaches to 18, as marked by the vertical dashed curve on the right-hand side of Fig. D2. This is because the maximum number of charging facilities needed is 18 when battery management is considered in the optimization framework, and the number is 12 in the other scenario, see Fig. 8 in Section 6. Then, the lifecycle cost of BEB fleet in both scenarios (with and without considering battery aging) as well as their difference would stay the same if the capacity of charging facilities exceeds 18. We note that, the threshold value $\bar{\gamma}$ is no smaller than 0.16 and may be up to 0.51 when the charging facilities are relatively enough. However, currently, the expected annual reduction rate of battery cost is less than 0.15 (Lutsey and Nicholas, 2019). Therefore, incorporating battery management into BEB scheduling can bring a certain number of cost saving from both short-term and long-term perspective. These further verify the significant practical values of battery management.

References

Addis, B., Carello, G., Ceselli, A., 2012. Exactly solving a two-level location problem with modular node capacities. Networks 59 (1), 161–180.

Adler, J.D., Mirchandani, P.B., 2014. Online routing and battery reservations for electric vehicles with swappable batteries. Transp. Res. Part B: Methodol. 70, 285–302.

An, K., 2020. Battery BEB infrastructure planning under demand uncertainty. Transp. Res. Part C: Emerg. Technol. 111, 572–587.

Bie, Y., Xiong, X., Yan, Y., Qu, X., 2020. Dynamic headway control for high-frequency bus line based on speed guidance and intersection signal adjustment. Comput.-Aided Civ. Infrastruct. Eng. 35 (1), 4–25.

Chediak, M., 2018. BEBs will take over half the world fleet by 2025. Available: https://www.bloomberg.com/news/articles/2018-02-01/electricbuses-will-take-over-half-the-world-by-2025.

Desrochers, M., Soumis, F., 1989. A column generation approach to the urban transit crew scheduling problem. Transp. Sci. 23 (1), 1–13.

Garey, M.R., Johnson, D.S., 1979. Computers and intractability, vol. 174. Freeman, San Francisco.

Gao, Z., Lin, Z., LaClair, T.J., Liu, C., Li, J.M., Birky, A.K., Ward, J., 2017. Battery capacity and recharging needs for electric buses in city transit service. Energy 122, 588–600.

Ghamami, M., Zockaie, A., Nie, Y.M., 2016. A general corridor model for designing plug-in electric vehicle charging infrastructure to support intercity travel. Transp. Res. Part C: Emerg. Technol. 68, 389–402.

Grolleau, S., Delaille, A., Gualous, H., Gyan, P., Revel, R., Bernard, J., Redondo-Iglesias, E., Peter, J., Network, S.I.M.C.A.L., 2014. Calendar aging of commercial graphite/LiFePO₄ cell–Predicting capacity fade under time dependent storage conditions. J. Power Sources 255, 450–458.

Gu, Y., Fu, X., Liu, Z., Xu, X., Chen, A., 2020. Performance of transportation network under perturbations: Reliability, vulnerability, and resilience. Transp. Res. Part E: Logist. Transp. Rev. 133, 101809.

Hiermann, G., Puchinger, J., Ropke, S., Hartl, R.F., 2016. The electric fleet size and mix vehicle routing problem with time windows and recharging stations. Eur. J. Oper. Res. 252 (3), 995–1018.

Hof, J., Schneider, M., Goeke, D., 2017. Solving the battery swap station location-routing problem with capacitated electric vehicles using an AVNS algorithm for vehicle-routing problems with intermediate stops. Transp. Res. Part B: Methodol. 97, 102–112.

Kang, Q., Wang, J., Zhou, M., Ammari, A.C., 2015. Centralized charging strategy and scheduling algorithm for electric vehicles under a battery swapping scenario. IEEE Trans. Intell. Transp. Syst. 17 (3), 659–669.

Keskin, M., Çatay, B., 2016. Partial recharge strategies for the electric vehicle routing problem with time windows. Transp. Res. Part C: Emerg. Technol. 65, 111–127.

Kim, M.E., Schonfeld, P., 2013. Integrating bus services with mixed fleets. Transp. Res. Part B: Methodol. 55, 227–244.

Lajunen, A., 2018. Lifecycle costs and charging requirements of electric buses with different charging methods. J. Cleaner Prod. 172, 56–67.

Lam, L., Bauer, P., 2012. Practical capacity fading model for Li-ion battery cells in electric vehicles. IEEE Trans. Power Electron. 28 (12), 5910–5918.

Lebeau, P., Macharis, C., Van Mierlo, J., 2016. Exploring the choice of battery electric vehicles in city logistics: A conjoint-based choice analysis. Transp. Res. Part E: Log. Transp. Rev. 91, 245–258.

Li, J.Q., 2013. Transit bus scheduling with limited energy. Transp. Sci. 48 (4), 521–539.

Li, J.Q., 2016. Battery-electric transit bus developments and operations: A review. Int. J. Sustain. Transp. 10 (3), 157–169.

Li, L., Lo, H.K., Xiao, F., Cen, X., 2018. Mixed bus fleet management strategy for minimizing overall and emissions external costs. Transp. Res. Part D: Transport and Environment 60, 104–118.

Liu, W., 2013. Introduction to Hybrid Vehicle System Modeling and Control. John Wiley & Sons, New Jersey, United States.

Lu, X., Sun, K., Guerrero, J.M., Vasquez, J.C., Huang, L., 2013. State-of-charge balance using adaptive droop control for distributed energy storage systems in DC microgrid applications. IEEE Trans. Ind. Electron. 61 (6), 2804–2815.

Lutsey, N., Nicholas, M., 2019. Update on electric vehicle costs in the United States through 2030. Int. Counc. Clean Transp 1–12.

Marra, F., Yang, G.Y., Træholt, C., Larsen, E., Rasmussen, C.N., You, S., 2012. Demand profile study of battery electric vehicle under different charging options. In: 2012 IEEE Power and Energy Society General Meeting. IEEE, pp. 1–7.

Masmoudi, M.A., Hosny, M., Demir, E., Genikomsakis, K.N., Cheikhrouhou, N., 2018. The dial-a-ride problem with electric vehicles and battery swapping stations. Transp. Res. Part E: Log. Transp. Rev. 118, 392–420.

Montoya, A., Guéret, C., Mendoza, J.E., Villegas, J.G., 2016. A multi-space sampling heuristic for the green vehicle routing problem. Transp. Res. Part C: Emerg. Technol. 70, 113–128.

Montoya, A., Guéret, C., Mendoza, J.E., Villegas, J.G., 2017. The electric vehicle routing problem with nonlinear charging function. Transp. Res. Part B: Methodol. 103, 87–110.

Nie, Y.M., Ghamami, M., Zockaie, A., Xiao, F., 2016. Optimization of incentive polices for plug-in electric vehicles. Transp. Res. Part B: Methodol. 84, 103–123.

Nykvist, B., Nilsson, M., 2015. Rapidly falling costs of battery packs for electric vehicles. Nat. Clim. Change 5 (4), 329–332.

Pelletier, S., Jabali, O., Laporte, G., Veneroni, M., 2017. Battery degradation and behaviour for electric vehicles: Review and numerical analyses of several models. Transp. Res. Part B: Methodol. 103, 158–187.

Pelletier, S., Jabali, O., Mendoza, J.E., Laporte, G., 2019. The BEB fleet transition problem. Transp. Res. Part C: Emerg. Technol. 109, 174–193.

Qin, N., Gusrialdi, A., Brooker, R.P., Ali, T., 2016. Numerical analysis of BEB fast charging strategies for demand charge reduction. Transp. Res. Part A: Policy and Practice 94, 386–396.

Qu, X., Wang, S., 2021. Communications in Transportation Research: Vision Scope. Commun. Transp. Res. 1, 100001.

Qu, X., Yu, Y., Zhou, M., Lin, C.T., Wang, X., 2020. Jointly dampening traffic oscillations and improving energy consumption with electric, connected and automated vehicles: A reinforcement learning based approach. Appl. Energy 257, 114030.

Rinaldi, M., Picarelli, E., D'Ariano, A., Viti, F., 2019. Mixed-fleet single-terminal bus scheduling problem: Modelling, solution scheme and potential applications. Omega. 102070.

Schneider, M., Stenger, A., Goeke, D., 2014. The electric vehicle-routing problem with time windows and recharging stations. Transp. Sci. 48 (4), 500–520.

Schoch, J., Gaerttner, J., Schuller, A., Setzer, T., 2018. Enhancing electric vehicle sustainability through battery life optimal charging. Transp. Res. Part B: Methodol. 112, 1–18.

Skog, K., Arbresparr, E., 2017. Svensk författningssamling, sfs 2017:1341, förordning om ändring i förordningen (2016:836) om elbusspremie. Available. http://www.energimyndigheten.se/globalassets/klimatmiljo/transporter/elbusspremien/forandringar-i-forordning-elbusspremie-sfs-20171341.

Wang, K., Zhen, L., Wang, S., Laporte, G., 2018. Column generation for the integrated berth allocation, quay crane assignment, and yard assignment problem. Transp. Sci. 52 (4), 812–834.

Wang, Y., Huang, Y., Xu, J., Barclay, N., 2017. Optimal recharging scheduling for urban BEBs: A case study in Davis. Transp. Res. Part E: Log. Transp. Rev. 100, 115–132.

Wen, M., Linde, E., Ropke, S., Mirchandani, P., Larsen, A., 2016. An adaptive large neighborhood search heuristic for the electric vehicle scheduling problem. Comput. Oper. Res. 76, 73–83.

Xu, M., Meng, Q., 2019. Fleet sizing for one-way electric carsharing services considering dynamic vehicle relocation and nonlinear charging profile. Transp. Res. Part B: Methodol. 128, 23–49.

Yi, Z., Smart, J., Shirk, M., 2018. Energy impact evaluation for eco-routing and charging of autonomous electric vehicle fleet: Ambient temperature consideration. Transp. Res. Part C: Emerg. Technol. 89, 344–363.

Zhang, Y., Xiong, R., He, H., Qu, X., Pecht, M., 2019. State of charge-dependent aging mechanisms in graphite/Li(NiCoAl)O_2 cells: Capacity loss modeling and remaining useful life prediction. Appl. Energy 255, 113818.